catalysts

MDPI

Article

C-H versus C-O Addition: A DFT Study of the Catalytic Cleavage of the β-O-4 Ether Linkage in Lignin by Iridium and Cobalt Pincer Complexes

Mary Mensah [1], Richard Tia [1], Evans Adei [1,*] and Nora H. de Leeuw [2,3,*]

[1] Department of Chemistry, Kwame Nkrumah University of Science and Technology, Kumasi 1916, Ghana; ajuablak@yahoo.com (M.M.); richtiagh@yahoo.com (R.T.)
[2] School of Chemistry, Cardiff University, Main Building, Park Place, Cardiff CF10 3AT, UK
[3] School of Chemistry, University of Leeds, Leeds LS2 9JT, UK
* Correspondence: eadei@yahoo.com (E.A.); n.h.deleeuw@leeds.ac.uk (N.H.d.L.)

Abstract: The potential energy surfaces of the reactions involved in the catalytic cleavage of *2*-phenoxy-*1*-phenylethanol, a model of the β-O-4 linkage in lignin, by (^{ipr}PCP)-Ir, (^{ipr}PCOP)-Ir, (^{ipr}PCP)-Co and (^{ipr}PCOP)-Co complexes have been studied using the M06/6-311G**/LANL2TZ level of theory. Both iridium and cobalt are found to be active towards the cleavage of the β-O-4 linkage, with rate constants of 44.7 s^{-1} and 5.1 × 10^6 s^{-1}, respectively. The iridium catalysts prefer the 'initial C-H addition' pathway, showing a kinetic preference of 16.8 kcal mol^{-1} over the 'direct C-O insertion' pathway, while the cobalt catalysts prefer the 'direct C-O insertion' route which is kinetically favored by 15.7 kcal mol^{-1} over the 'initial C-H addition' pathway. A two-state reactivity occurs along the preferred pathway for the cobalt-catalyzed reaction.

Keywords: pincer complexes; homogenous catalysis; C-O bond cleavage; oxidative addition lignin valorization

check for updates

Citation: Mensah, M.; Tia, R.; Adei, E.; de Leeuw, N.H. C-H versus C-O Addition: A DFT Study of the Catalytic Cleavage of the β-O-4 Ether Linkage in Lignin by Iridium and Cobalt Pincer Complexes. *Catalysts* **2023**, *13*, 757. https://doi.org/10.3390/catal13040757

Academic Editors: Elisabete Alegria, Andreia F. Peixoto and Mohamed M. A. Soliman

Received: 8 March 2023
Revised: 9 April 2023
Accepted: 12 April 2023
Published: 15 April 2023

Copyright: © 2023 by the authors. Licensee MDPI, Basel, Switzerland. This article is an open access article distributed under the terms and conditions of the Creative Commons Attribution (CC BY) license (https://creativecommons.org/licenses/by/4.0/).

1. Introduction

The mono-anionic ECE-type pincer systems are very common due to their comparative ease of synthesis. Known to be planar with a single aromatic backbone, they possess a central aryl anionic carbon 'C' and ortho substituents bearing side arm donor groups 'E', where E is N or P. These pincer ligands make up an attractive niche of ligand frameworks that provide a suitable balance between stability and reactivity and have become widely used in homogenous catalysis [1]. For example, the complex (PCP)Ir (PCP = κ3-C_6H_3-2,6-[$CH_2P(t\text{-}Bu)_2$]$_2$) and its derivatives are known as the most effective alkane dehydrogenation catalysts developed to date [2–4]. Pincer complexes have also been shown to be catalytically active in the activation of C-X bonds (X = C, O, N, F etc.). In 2008, Chirik et al. reported the cleavage of C-O bonds in alkyl-substituted esters via binuclear oxidative addition using (^{ipr}PDI)Fe(N_2)$_2$ (Scheme 1) [5]. Other noteworthy examples of sp^3 C-O bond cleavage include the rearrangement reactions of methyl aryl ethers by a tris(pyrazolyl)borate iridium complex reported by Carmona and Paneque [6–8], as well as reports by Ozerov and Grubbs on the cleavage of the tert-butyl-oxygen and benzyl-oxygen bonds of methyl ethers by a PNP-pincer iridium complex [9]. Recently, Choi et al. [10] reported the oxidative addition of C(sp^3-O) bonds of methyl esters, methyl tosylate and methyl aryl ethers using (PCP)Ir (PCP = κ3-C_6H_3-2,6-[$CH_2P(t\text{-}Bu)_2$]$_2$).

These reports highlight some of the progress that has been made in addressing the challenges associated with the catalytic activation of sp^3 C-O bonds, one of the primary linkages in organic chemistry. The activation of these types of C-O bonds is also a focus area of interest for the catalytic valorization of lignin to deoxygenated fuels and commercial chemicals. Lignin, which makes up 40% of the weight of biomass, is mostly comprised

of alkyl aryl ether bonds that are difficult to break due to their strength and stability. Current research focuses on understanding how the β-O-4 linkage, which is the most abundant linkage in lignin, can be cleaved [11]. In 2014, Haibach et al. reported the dehydroaryloxylation of alkyl aryl ethers using PCP-type iridium complexes [12], making it the second report of this type of cleavage reaction being undertaken in a fully atom-economic fashion, following in investigations carried out by Bergman et al. [13] A previous study conducted by Haibach et al. on the formation of ether C-O bonds through the same PCP-type iridium-catalyzed olefin hydroaryloxylation [14] led to their 2014 investigation after they discovered that the catalyst could also carry out the reverse reaction, i.e., 'ether dehydroaryloxylation'. From the optimization studies carried out by Haibach et al. [12], the use of less sterically bulky precursors (^{ipr}PCP)Ir **A** and (^{ipr}PCOP)Ir **B** (Scheme 2) was found to be beneficial as they led to much higher conversions.

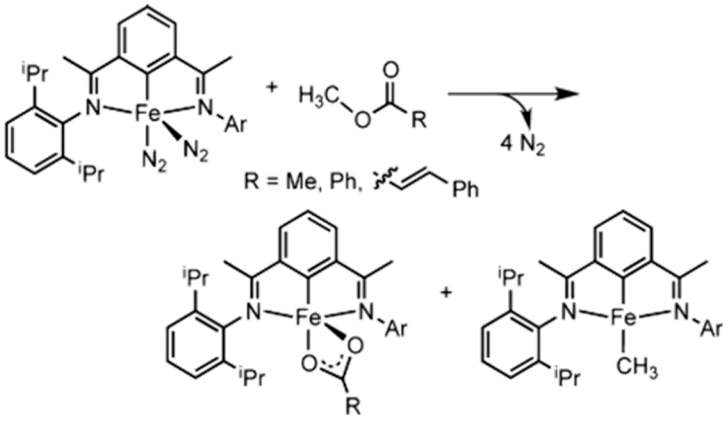

Scheme 1. Cleavage of C-O bonds in alkyl-substituted esters using (^{ipr}PDI)Fe(N_2)$_2$. Study carried out by Chirik et al.

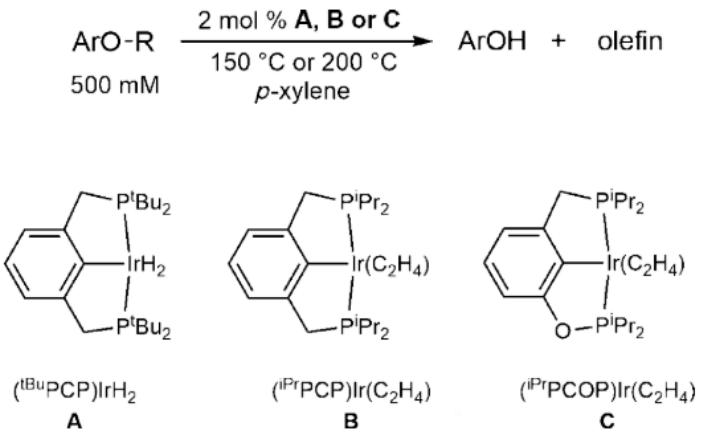

Scheme 2. Dehydroaryloxylation of aryl ethers using PCP-type iridium complexes. Study carried out by Haibach et al.

However, it is still not understood from a mechanistic point of view how these bonds are cleaved. In studies carried out by Choi et al., both DFT calculations and experimental work have shown that the C-O bond cleavage proceeded via initial C-H bond activation rather than the direct C-O insertion [10]. Aryl C-H insertion was also observed to be kinetically favored in the reaction of $RuH_2CO(PPH_3)$ with aryl ethers [15]. However, DFT studies backed by experimental findings reported by Chmely et al. showed the kinetic preference of the direct C-O activation over C-H activation in the cleavage of an alkyl aryl ether using a Ru-xantphos catalyst [16]. Liu and Wilson also reported a DFT study on the reaction between PCP-type group 8 complexes with a model of the β-O-4 linkage in lignin, where the reaction proceeds via direct C-O bond cleavage [17]. Consequently, in the effort

to develop an efficient pincer-type catalyst for the cleavage of the alkyl–aryl ether bonds in lignin, the question of whether the reaction proceeds via initial C-H bond activation or via direct C-O bond insertion needs to be resolved.

Inspired by the work by Haibach and coworkers [11], here we report an exploratory mechanistic study on the catalytic activity of (^{ipr}PCP)Ir and (^{ipr}PCOP)Ir towards the cleavage of the β-O-4 linkage, 2-phenoxy-*1*-phenyl-ethanol (Scheme 3). We have investigated the energetics (kinetics and thermodynamics) of the reaction along three proposed pathways (Schemes 1–3) to determine whether the C-O bond cleavage proceeds via initial C-H activation or via direct C-O bond insertion. For comparison, we have also investigated the catalytic activity of (^{ipr}PCP)Co and (^{ipr}PCOP)Co for the cleavage reaction and compared the energetics with that of the iridium-catalyzed reaction. Cobalt-based pincer-type complexes are a relatively cheap and abundant alternative for catalytic applications, which have been applied successfully in a variety of dehydrogenation and hydrogenation reactions [18].

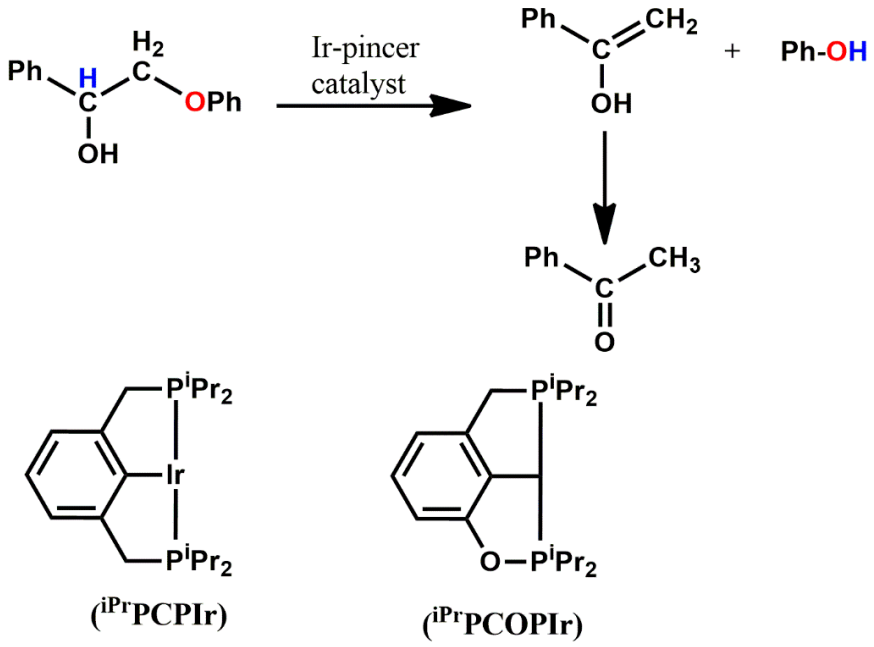

Scheme 3. Chemical equation for the catalytic cleavage of the β-O-4 linkage, 2-phenoxy-*1*-phenyl-ethanol using PCP-type iridium complexes and the chemical structures of the catalysts used.

Scheme 4 shows the mechanistic pathway as proposed by Haibach et al. (route A). The initial step is the addition of the α-C-H bond to the metal center to yield **A2**, followed by the C-O insertion step to form the six-coordinate Ir intermediate **A3**. Loss of the phenol **5** and enolate **6**, which rearranges to the more stable acetophenone **7**, regenerates the Ir-pincer active species and completes the catalytic cycle.

The second mechanism as proposed by Liu and Wilson [17] begins with the coordination of the ether oxygen to the metal center to form an adduct. Direct C-O bond addition follows to form the five-coordinate intermediate **B3**, followed by the α-C-H bond addition to form **B4**. Finally, the phenol and enolate, which rearrange to acetophenone, are released to regenerate the Ir-pincer active species, as shown in Scheme 5.

The third proposed reaction pathway, shown in Scheme 6, is similar to the mechanism proposed by Wu et al. [19] in their experimental study of the cleavage of a β-O-4 model compound using a Ru-xantphos catalyst. It begins with dehydrogenation of the substrate 2-phenoxy-*1*-phenyl-ethanol **1** to its corresponding ketone motif **C2**. **C2** undergoes rearrangement via **TSC1** to a slightly more stable adduct with a three-membered ring formed between the ketone carbon, the ketone oxygen and the Ir center. This is followed by the direct C-O bond insertion to form **C4**, which undergoes hydrogenation using the H_2 generated earlier. The H_2 molecule, which binds to the metal to form a dihydrogen complex

C5, is used in the subsequent reductive elimination of phenol and acetophenone and the Ir-pincer catalyst is regenerated to repeat the catalytic cycle.

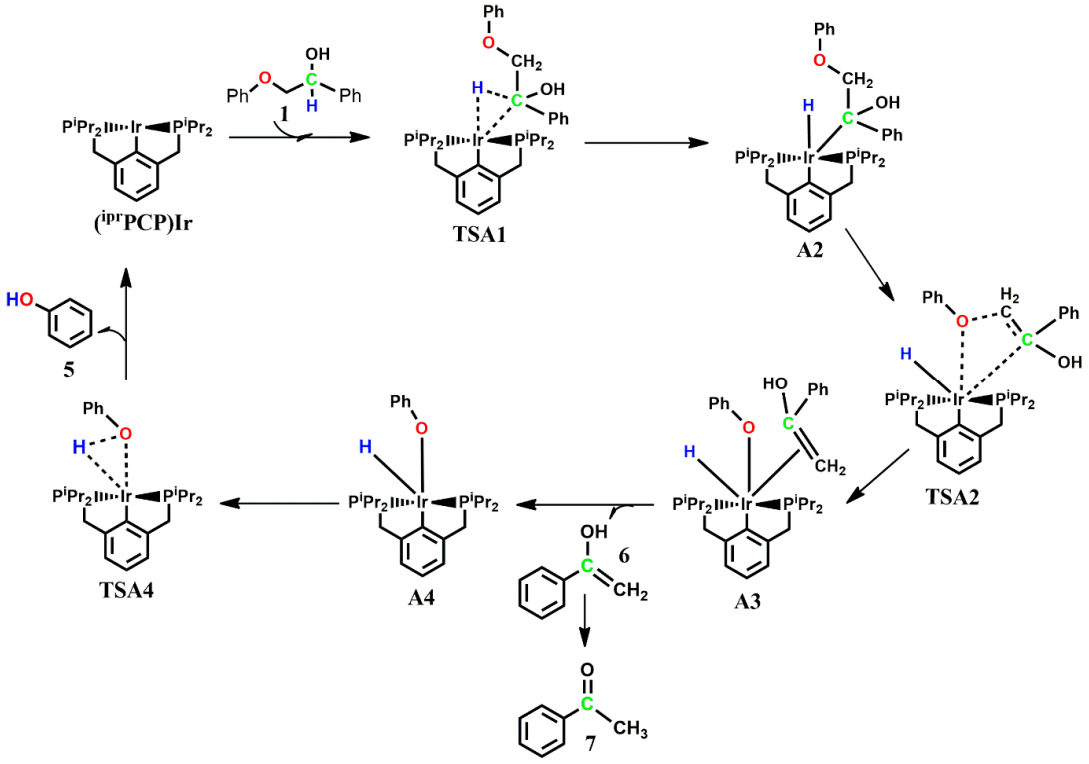

Scheme 4. Proposed mechanism for the cleavage 2-phenoxy-*1*-phenyl-ethanol by pincer complexes along pathway A.

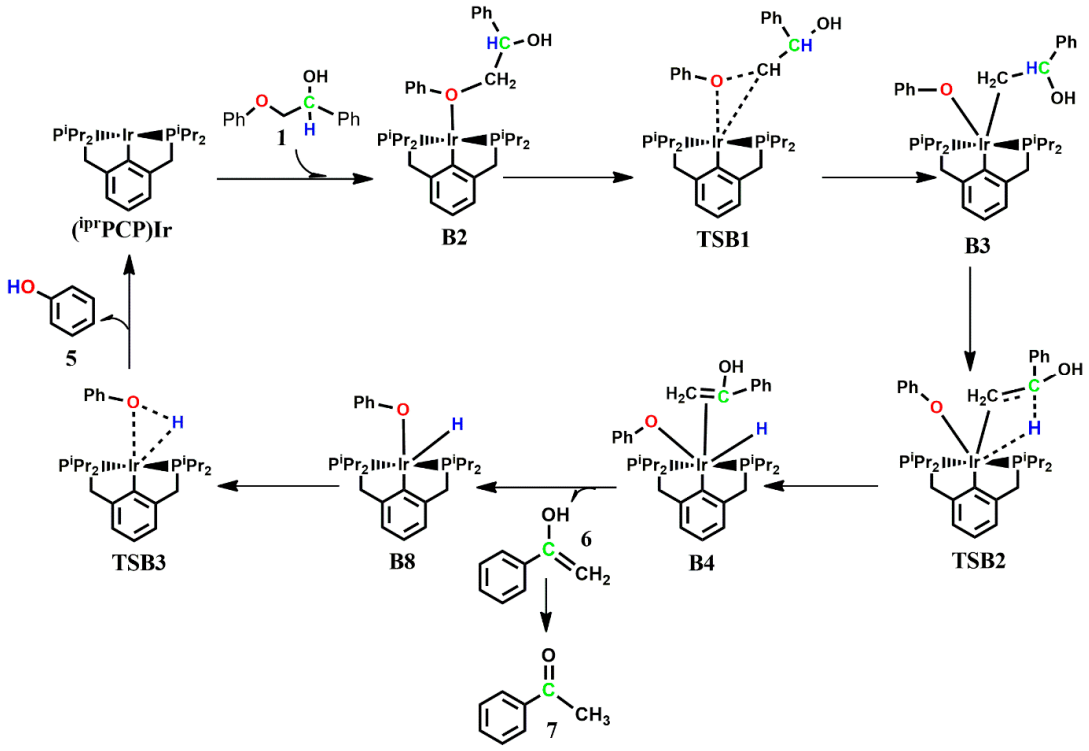

Scheme 5. Proposed mechanism for the cleavage 2-phenoxy-*1*-phenyl-ethanol by pincer complexes along pathway B.

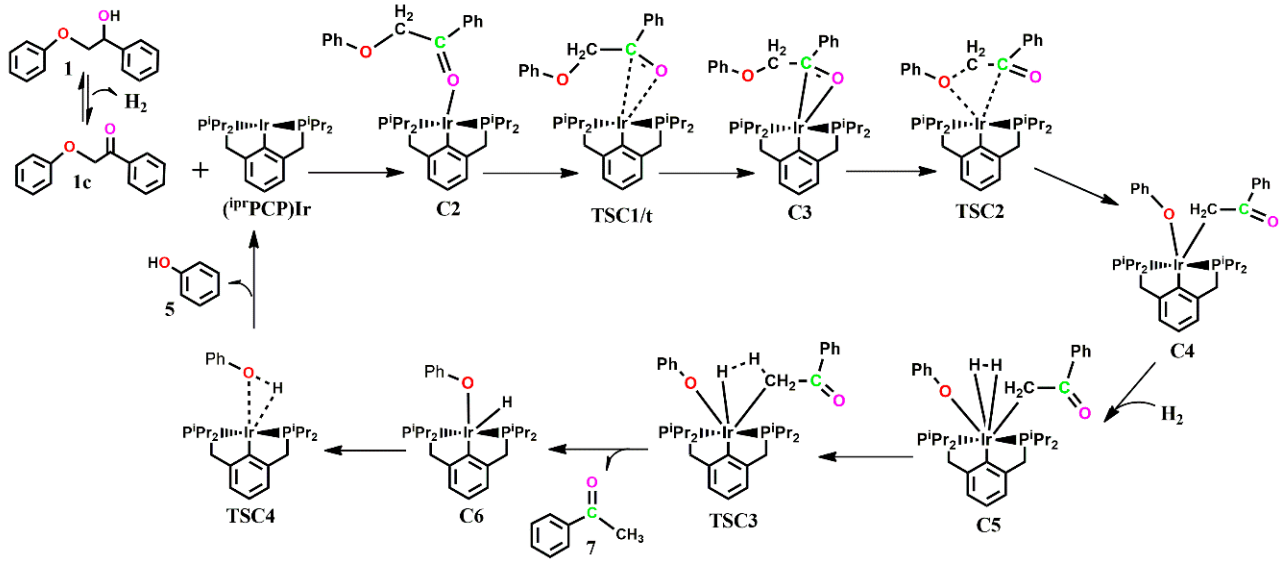

Scheme 6. Proposed mechanism for the cleavage 2-phenoxy-*1*-phenyl-ethanol by pincer complexes along pathway C.

2. Results and Discussion

2.1. The Reaction of (ipr PCP)Ir with 2-Phenoxy-1-phenylethanol **1**

The optimized geometries of the stationary points, as well as the Gibbs free energy profile for the reaction of **(*ipr*PCP)Ir** with 2-phenoxy-*1*-phenylethanol **1** along path **A** are shown in Figures 1 and 2. All stationary points in the catalytic cycle were sought on both the singlet and triplet state potential energy surface (PES), but triplet-state energies were found to be highly unstable, with the reactants being 104 kcal mol^{-1} less stable on the triplet surface than on the singlet surface (Table 1).

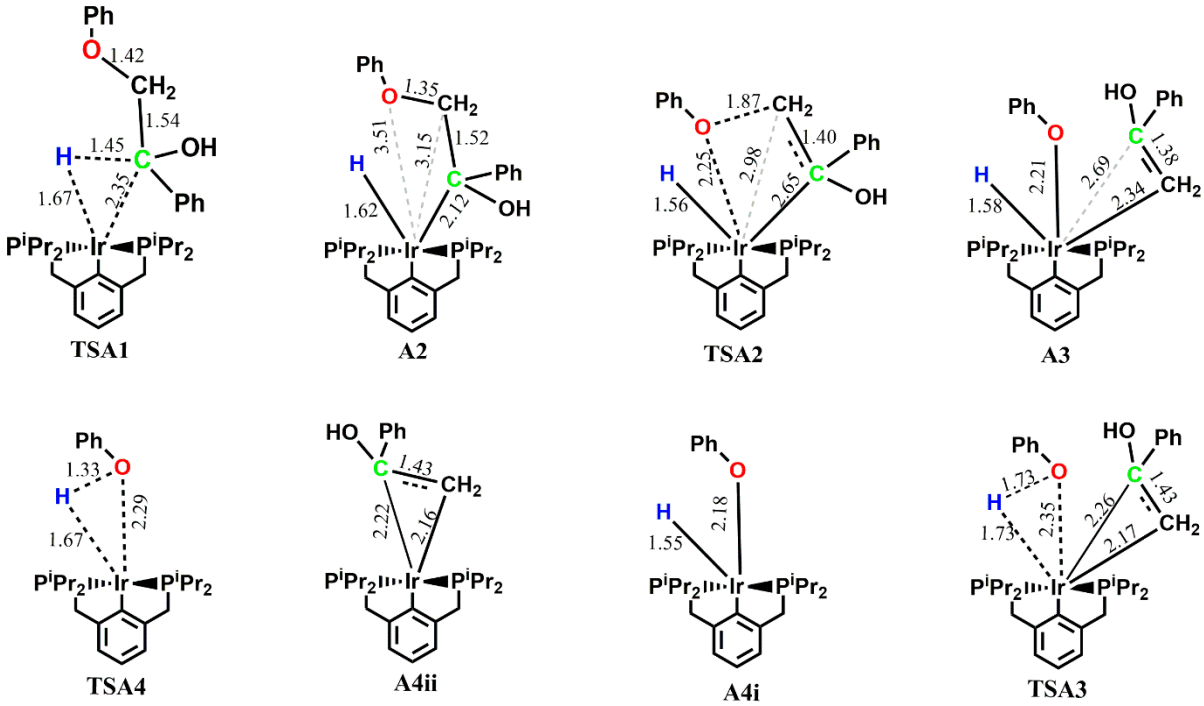

Figure 1. Optimized geometries of the main stationary points involved in the reaction of **(*ipr*PCP)Ir** with 2-phenoxy-*1*-phenylethanol **1** along pathway A. Distances in Å.

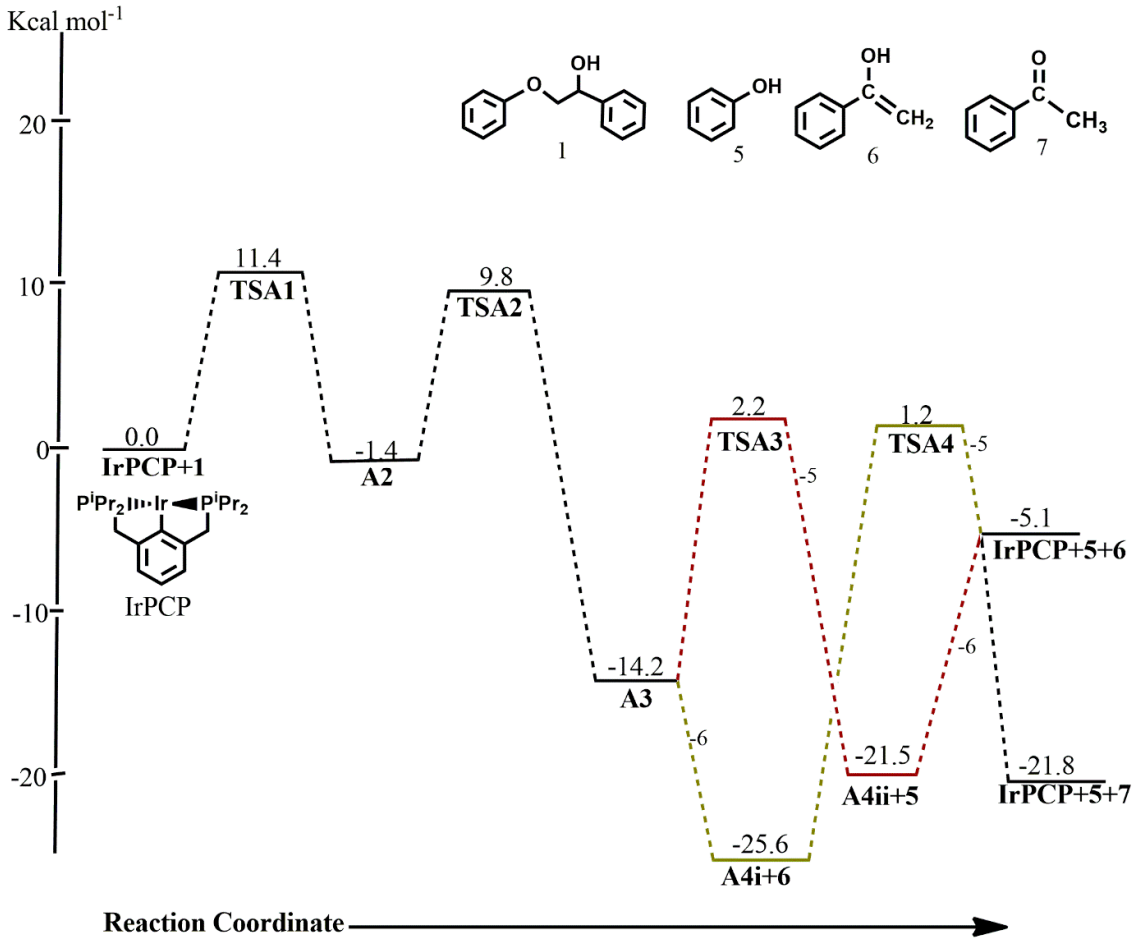

Figure 2. Free energy landscape of the overall catalytic cycle for the reaction of **(^{ipr}PCP)Ir** with **1** along pathway A.

Table 1. Comparison of singlet-state and triplet-state energies of the stationary points involved in the reaction of **(^{ipr}PCP)Ir** with **1** along path A.

	Singlet State/Kcal mol^{-1}	Triplet State/Kcal mol^{-1}
IrPCP+1	0.0	106.8
TSA1	11.4	34.2
A2	−1.4	19.7
TSA2	9.8	Could not be located
A3	−14.2	Could not be located
TSA3	2.3	14.1
A4i+6+7	−25.6	57.9
A4ii+5	−21.5	96.9
TSA4	1.2	86.0
IrPCP+5+6	−5.1	166.4
IrPCP+5+7	−21.8	168.6

The first step in pathway A, which is the C-H addition, proceeds with an activation energy barrier of 11.4 kcal mol^{-1}, leading to a five-coordinate complex **A2**. Both the hydrogen being extracted by the metal and the β-O-4 group sit axially to the pincer backbone in **TSA1**, and the transition state is a three-membered structure involving the

α-carbon, the corresponding hydrogen and the metal. The Ir-C bond in the three-membered structure transitions from a bond length of 2.35 Å in **TSA1** to 2.12 Å in **A2** ($d_{Ir\text{-}C}$ = 2.12 Å) and both the abstracted hydrogen and the β-O-4 compound retain their axial position in **A2**. On the triplet PES, the activation energy barrier for the C-H addition is 34.1 kcal mol^{-1} and the resulting triplet intermediate is 21.1 kcal mol^{-1} less stable than the singlet state intermediate. The next step, which is the insertion of the ether C-O bond for subsequent cleavage to the metal center, proceeds via a four-membered transition state **TSA2** involving the metal, the α-carbon, the ether oxygen and the ether carbon, with an activation energy barrier of 11.2 kcal mol^{-1}. The bond between the iridium and the ether carbon transitions from having no significant interaction ($d_{Ir\text{-}C}$ = 3.15 Å) in **A2** to 2.34 Å in **A3**, with the O-Ir-C angle moving from 63.9° in **A2** to 92.2° in **TSA2** to 53.1° in **A3**. Triplet state structures for **TSA2** and **A3** were found not to exist on the reaction surface. In the six-coordinate intermediate (^{ipr}PCP)Ir(H)(OPh)(enolate) **A3**, the enolate which was proposed to form a π-complex with the metal center [14] preferably binds to the metal center via the methylene carbon in an equatorial fashion while the phenolate sits axially to the pincer backbone. The two possible orders of product release were considered, and it was revealed that the thermodynamic product is the enolate, which rearranges to the more stable ketone while the kinetic product is the phenol. On the singlet surface, the formation of **A4i** mixed with the free enolate **6**, which can rearrange to the more stable ketone **7**, is calculated to be the major resting state in the catalytic cycle with a free energy of −25.6 kcal mol^{-1} relative to the reactants, whereas **A4i** undergoes reductive elimination to give phenol with an activation barrier of 26.8 kcal mol^{-1}; this step is endergonic by 20.6 kcal mol^{-1}. In contrast, the release of phenol first proceeds with an activation barrier of 16.4 kcal mol^{-1} and the subsequent release of the catalyst is endergonic by 16.4 kcal mol^{-1}. An exhaustive search for the transition state from **A3** and **A4ii** that leads to the bond cleavage of the enolate and the release of the catalyst was not fruitful. The energies for both orders of product release show that subsequent removal of either the phenol or the enolate, which rearranges to the more stable ketone, to give back the catalyst is kinetically unfavorable. This means that the likely predominant products are **A4i+6+7** (the thermodynamic product) and **A4ii+5** (the kinetic product). These findings are consistent with reports from experimental work carried out by Kundu et al. where the intermediate prior to the release of phenol was isolated instead of the phenol and the catalyst [14]. On the triplet PES, the formation of the **A4i** is less stable than the singlet product by 83.5 kcal mol^{-1} while formation of **A4ii** is less stable by 118.1 kcal mol^{-1}. Although some of the minima (intermediates) and transition states in the catalytic cycle exist both in the singlet state and in the triplet state, the singlet state structures would deplete the triplet state reaction surface and no multiple-state reactivity is observed in the catalytic cycle.

The optimized geometries of the stationary points, as well as the Gibbs free energy profile for the reaction of **(^{ipr}PCP)Ir** with *2*-phenoxy-*1*-phenylethanol **1** along pathway **B** are shown in Figures 3 and 4. Triplet-state energies obtained along this pathway were also found to be less stable than the singlet-state energies (Table 2). The reaction begins with the ether oxygen coordinating axially to the metal center, which is exergonic by −6.9 kcal mol^{-1}, and a bond is formed between the Ir and O to give **B2**, which was not found to exist on the triplet surface. Subsequent addition of the *β*-carbon to Ir and cleavage of the ether C-O bond takes place with an activation energy barrier of 34.1 kcal mol^{-1}.

Here, the C-O bond insertion proceeds via a three-membered transition state **TSB1**, leading to the five-coordinate intermediate **B3**, which is exergonic by 10.5 kcal mol^{-1}. The Ir-O bond length transitions from a bond length of 2.32 Å in **B2** to 2.23 Å in **B3**, while the phenolate remains axial to the pincer backbone and the enolate sits in an equatorial fashion. The Ir-C(H_2) bond also moves from having no significant interaction ($d_{Ir\text{-}C}$ = 3.32 Å) in **B2** to a covalent bond ($d_{Ir\text{-}C}$ = 2.08 Å) in **B3**. The intermediate **B3** was also located on the triplet PES, but was found to be less stable by 19.6 kcal mol^{-1}, while the transition state leading to **B3** was found not to exist on the triplet surface. Subsequent H abstraction by Ir from the α-carbon proceeds via a four-membered early transition state **TSB2** with an

activation energybarrier of 22.5 kcal mol^{-1}, leading to a six-Ir-coordinated complex **B4i**. In the intermediate **B4i**, the enolate sits axially to the aromatic backbone of the pincer ligand, forming a π-complex with the iridium center and moving the phenolate and the abstracted hydrogen to the equatorial position. Neither **TSB2** nor **B4** could be located on the triplet potential energy surface. In order to determine the preferred order of product release, a different isomer of **B4i** which would allow for the release of the phenol first was located on the PES, but this isomer **B4ii** was found to be less stable by 12.4 kcal mol^{-1} than **B4i**.

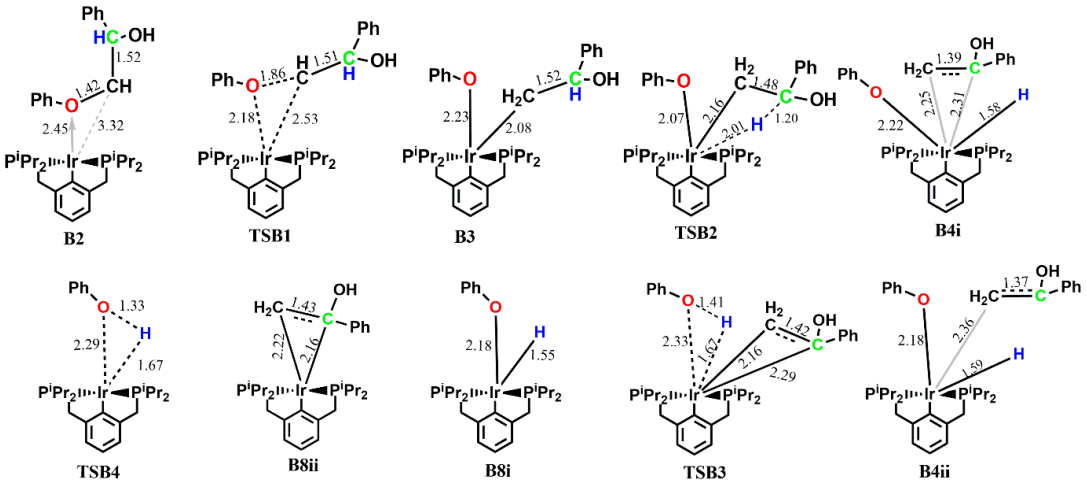

Figure 3. Optimized geometries of the main stationary points involved in the reaction of (**^{ipr}PCP)Ir** with 2-phenoxy-*1*-phenylethanol **1** along pathway B. Distances in Å.

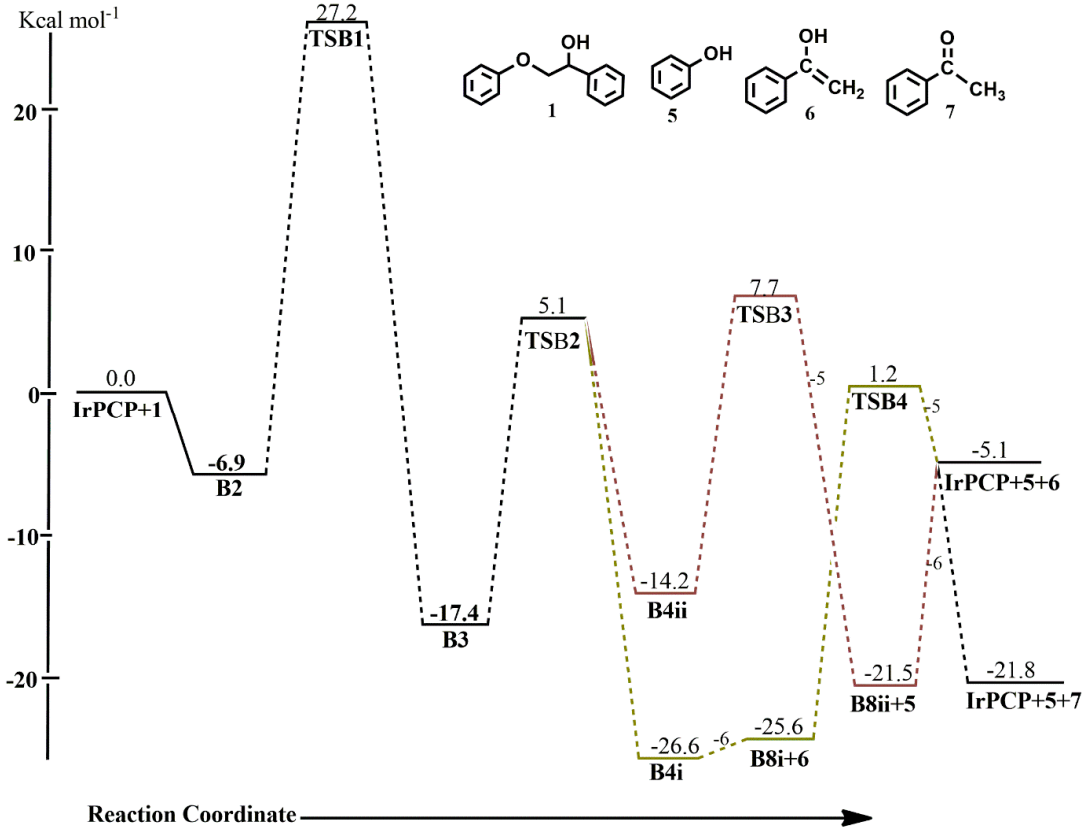

Figure 4. Free energy landscape for the overall catalytic cycle for the reaction of (**^{ipr}PCP)Ir** with **1** along pathway **B**.

Table 2. Comparison of singlet-state and triplet-state energies of the stationary points involved in the reaction of **(^{ipr}PCP)Ir** with **1** along path B.

	Singlet State/Kcal mol^{-1}	Triplet State/Kcal mol^{-1}
IrPCP+1	0.0	106.8
B2	−6.9	Could not be located
TSB1	27.2	Could not be located
B3	−17.4	2.2
TSB2	5.1	Could not be located
B4i	−26.6	Could not be located
B4ii	−14.2	Could not be located
TSB3	7.7	86.0
B8i+6+7	−25.6	57.9
TSB4	1.2	86.0
B8ii+5	−21.5	96.9
IrPCP+5+6	−5.1	166.4
IrPCP+5+7	−21.8	168.6

The corresponding activation barrier for the initial release of the phenol from the predominant isomer of **B4i** is 34.3 kcal mol^{-1}. Initial release of the enolate proceeds without barrier via the bond cleavage of the η^2-Ir-C bond in a slightly endergonic fashion (ΔG° = 1.0 kcal mol^{-1}), followed by the release of phenol which proceeds with an activation barrier of 26.8 kcal mol^{-1} and is endergonic by 20.5 kcal mol^{-1}. This shows that the preferred order of product release is the initial release of the enolate followed by the release of the phenol. However, the energetics also show that the predominant product is **B8i+6+7**, as subsequent release of the phenol and the catalyst is shown to be kinetically less favored. Similar to pathway A, the formation of **B8** and the transition state structure for the release of phenol are highly unstable on the triplet PES, and the major product formed is the enolate **6** which rearranges to the acetophenone 7 (essentially 7), as shown in Figure 4. No multiple state reactivity is observed along path B.

The optimized geometries of the stationary points, as well as the Gibbs free energy profile for the reaction of **(^{ipr}PCP)Ir** with *2*-phenoxy-*1*-phenylethanol **1** along pathway **C** are shown in Figures 5 and 6. The reaction begins with the substrate binding to the catalyst via the ketone oxygen after undergoing dehydrogenative equilibrium in an exergonic fashion to give the adduct **C2**. **C2** is located both on the singlet and triplet surface, with the triplet state structure being less stable by 12.9 kcal mol^{-1} (Table 3). The complex **C2**, which is proposed to undergo direct C-O bond cleavage, rather undergoes initial rearrangement to form a π-complex across the ketone C-O bond to the Ir center, allowing the ether oxygen of the substrate to sit in a much closer proximity to the metal center to allow for subsequent C-O addition. This rearrangement is thermoneutral and proceeds via **TSC1**, which could only be located on the triplet PES with an activation barrier of 31.5 kcal mol^{-1}. Although the activation barrier for the formation of **C3** would be lower on the triplet surface, the more stable singlet-state **C2** would deplete the surface of the triplet-state **C2**, making the formation of **C3** proceed from singlet-state **C2** via triplet-state **TSC1** to singlet-state **C3**. The intermediate **C3** is also located on the triplet surface, but is found to be less stable by 30.4 kcal mol^{-1} than the singlet-state **C3**. Subsequent C-O bond cleavage follows via **TSC2**, which involves the ether oxygen, the ether carbon, α-carbon and the Ir, with an activation barrier of 26.7 kcal mol^{-1} to give a five-membered Ir-complex **C5**, containing the phenoxide and what should have been a π-complex between the C-C bond and the Ir, but which is

optimized as a C-bound ketone. The formation of **C4** is exergonic by 21.4 kcal mol^{-1} on the singlet PES while the triplet state **C4** is less stable by 20.4 kcal mol^{-1}. Coordination of initially released H_2 is exergonic by 3.2 kcal mol^{-1} leading to an η^2–H_2 complex **C5**, shown to be the major resting state in the kinetically preferred catalytic cycle. In **C5**, which is only located to the singlet PES, the H_2 ligand binds axially to the aromatic backbone of the pincer ligand while both the phenoxide and ketone are arranged equatorial to it, allowing for reductive elimination of either the phenol or the acetophenone. The release of the acetophenone first proceeds via **TSC3i** with a barrier of 24.1 kcal mol^{-1}, followed by the release of the phenol via **TSC4i** with a barrier of 26.7 kcal mol^{-1}, while the barriers for release of the phenol first, followed by subsequent release of the acetophenone, proceeding via **TSC3ii** and **TSC4ii**, are 19.2 kcal mol^{-1} and 4.5 kcal mol^{-1}, respectively. The formation of **C6i+7** from the initial release of the acetophenone is seen as the major resting state ($\Delta G = -41.8$ kcal mol^{-1}) in the reaction cycle, also showing that the acetophenone **7** would be the predominant product obtained, while the phenol **5** is the kinetic product. The release of the catalyst is also seen to be kinetically feasible if the pathway that follows the initial release of the phenol is considered. The η^2–H_2 complex **C5**, or the transition states **TS3i** and **TS3ii**, could not be located on the triplet PES, while the intermediates C6i and C6ii, as well as the transition states **TS4i** and **TS4ii** that were found on the triplet PES, were highly unstable. A two-state reactivity is observed along this pathway (path C) with the transition state for the rearrangement of **C2** to **C3** located only in the triplet state. However, the other stationary points on the catalytic cycle, which exist both on the singlet surface as well as on the triplet surface, show the singlet state structures to be the ground state structures of the system.

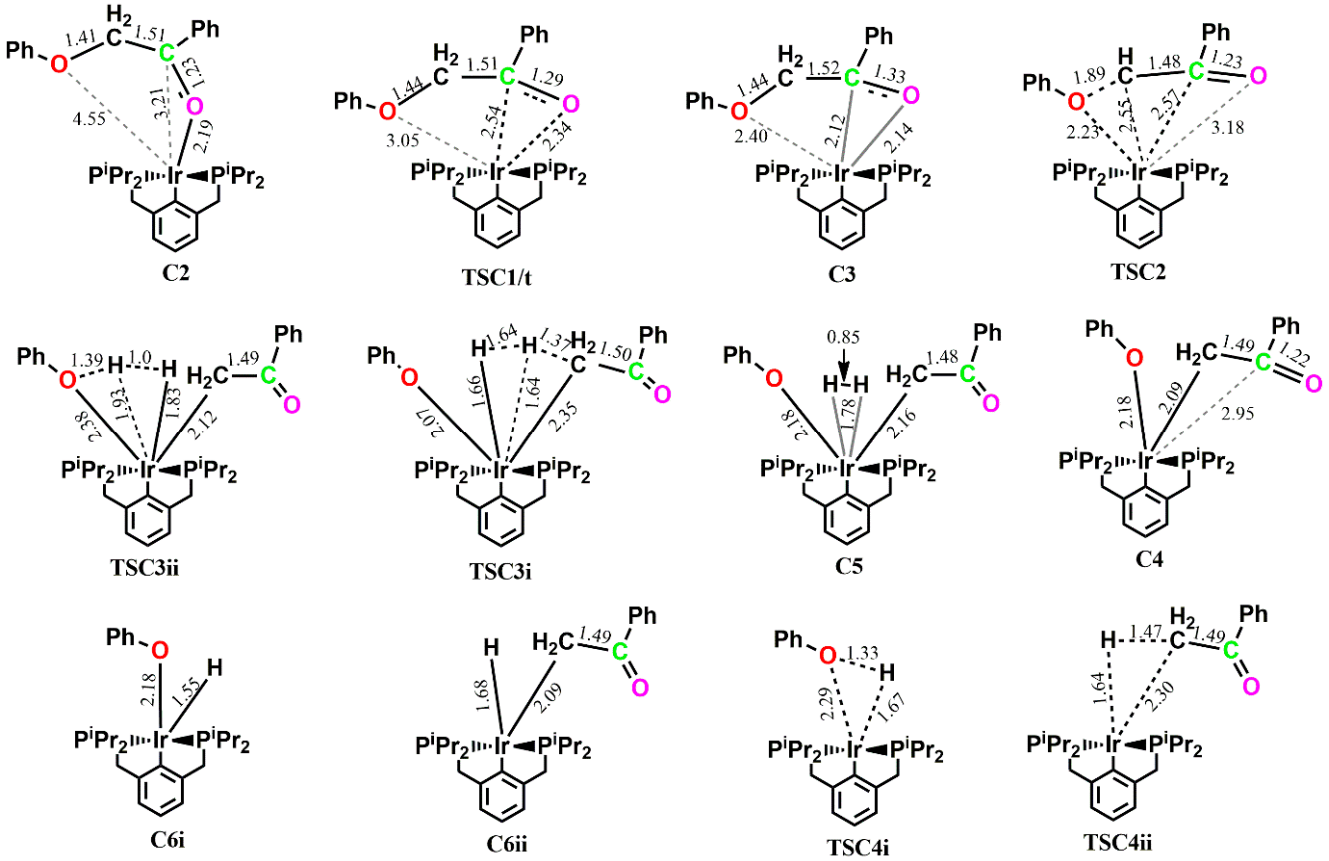

Figure 5. Optimized geometries of the main stationary points involved in the reaction of (^{ipr}**PCP)Ir** with 2-phenoxy-*1*-phenylethanol **1** along pathway C. Distances in Å.

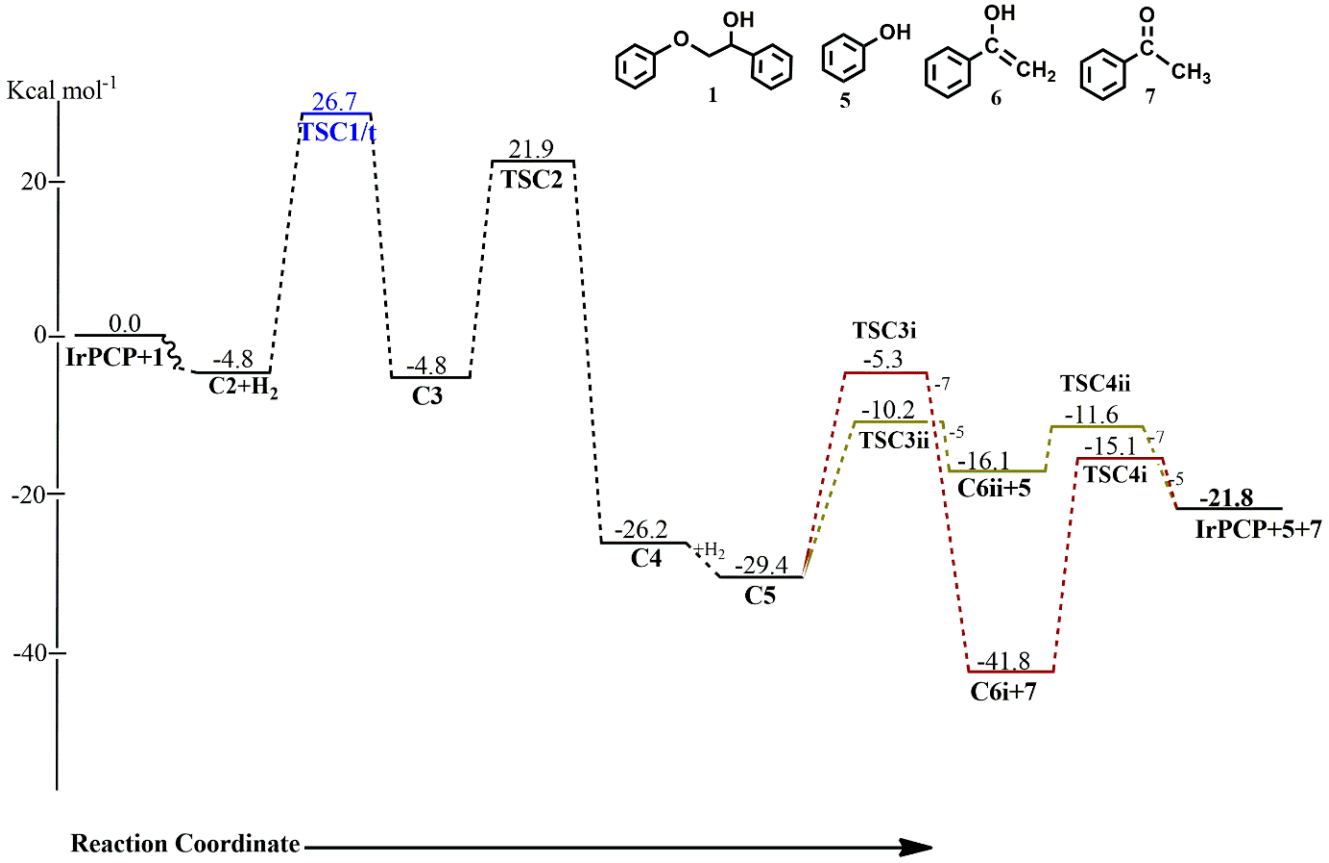

Figure 6. Free energy landscape for the overall catalytic cycle for the reaction of **(^{ipr}PCP)Ir** with **1** along pathway C. Triplet state energies shown in blue.

Table 3. Comparison of singlet-state and triplet-state energies of the stationary points involved in the reaction of **(^{ipr}PCP)Ir** with **1** along path C.

	Singlet State/Kcal mol^{-1}	Triplet State/Kcal mol^{-1}
IrPCP+1	0.0	106.8
C2	−4.8	8.1
TSC1	Could not be located	26.7
C3	−4.8	25.6
TSC2	21.9	24.3
C4	−26.2	−5.8
C5	−29.4	Could not be located
TSC3i	−5.3	Could not be located
TSC3ii	−10.2	Could not be located
C6i+7	−41.8	90.0
C6ii+5	−16.1	60.1
TSC4i	−15.1	120.2
TSC4ii	−11.6	88.2
IrPCP+5+7	−21.8	168.6

Tables 4–6 show comparisons in activation energies, energies of formation and apparent activation energies (δE) for the entire cycles calculated for the three pathways and for the two different ligand combinations. For pathway A, where the ether bond cleavage pro-

ceeds via the initial C-H addition, the δE was calculated to be 15.2 kcal mol^{-1}, while the δE for pathway B and pathway C, where ether bond cleavage proceeds via direct C-O bond addition, were calculated to be 32.0 kcal mol^{-1} and 27.0 kcal mol^{-1}, respectively. Taking into account preferred product outcomes, the δE for pathway A reduces to 11.1 kcal mol^{-1} when the phenol is the desired product, while the δE for pathway C increases to 46.7 kcal mol^{-1} when the acetophenone is the desired product. From these apparent activation energies, the selectivity for the initial C-H addition pathway for this type of cleavage reaction, as observed in studies carried out by Choi et al. [14] and Haibach et al. [13], has been demonstrated. The activation barrier for the ether bond cleavage is also lower in pathway A (Ea = 16.4 kcal mol^{-1}) than in pathways B (Ea = 34.1 kcal mol^{-1}) and C (Ea = 26.7 kcal mol^{-1}). For all three pathways, the phenol is observed as the kinetic product, while the enolate/acetophenone is observed as the thermodynamic product, and release of the catalyst becomes more kinetically feasible when phenol is the desired product. It should also be noted that for pathways B and C, in which the reaction proceeds via direct C-O bond addition, C-O bond cleavage in pathway C, which involves the presence of the ketone functionality of the substrate, is kinetically favored by 7.4 kcal mol^{-1} over pathway B. These results support both experimental [12] and theoretical [20] findings, which have reported that the presence of the ketone functionality facilitates the C-O bond cleavage and that the bond dissociation energy of the ketone is far less than its alcohol counterpart.

Table 4. Activation energies and reaction energies for the reaction of **1** with **[IrPCP]** and **[IrPOCP]** along path A. Energies in kcal mol^{-1}.

	EaA1	**ΔEA2**	**EaA2**	**ΔEA3**	**EaA3**	**ΔEA4i+5**	**ΔEA4i+6/7**	**EaA4**	**Δ*Gr***	**δ*E*(5)**
(^{ipr}PCP)Ir	11.4	−1.4	11.2	−12.8	16.4	−7.3	−11.4	26.8	−21.8	15.2
(^{ipr}PCOP)Ir	12.0	−2.5	22.3	−24.0	13.2	−9.1	−12.9	24.9	−21.8	16.7

Table 5. Activation energies and reaction energies for the reaction of **1** with [IrPCP] and [IrPOCP] along path B. Energies in kcal mol^{-1}.

	ΔEB2	**EaB1**	**ΔEB3**	**EaB2**	**ΔEB4i**	**ΔEB4ii**	**EaB3**	**ΔEB8i+6/7**	**EaB4**	**ΔEB8i+5**	**Δ*Gr***	**δ*E***
(^{ipr}PCP)Ir	−6.9	34.1	−10.5	22.5	−9.2	3.2	34.3	1.0	26.8	5.1	−21.8	32.0
(^{ipr}PCOP)Ir	−11.2	39.5	−5.8	22.7	−10.3	3.5	36.6	0.8	25.8	4.7	−21.8	33.8

Table 6. Activation energies and reaction energies for the reaction of **1** with **[IrPCP]** and **[IrPOCP]** along path C. Energies in kcal mol^{-1}.

	ΔEC2	**EaC1**	**ΔEC3**	**EaC2**	**ΔEC4**	**ΔEC5**	**EaC3i**	**EaC3ii**	**ΔEC6i+7**	**ΔEC6ii+5**	**EaC4i**	**EaC4ii**	**Δ*Gr***	**δ*E***
(^{ipr}PCP)Ir	−4.8	31.5	0.0	26.7	−21.4	−3.2	24.1	19.2	−12.4	13.3	26.7	4.5	−21.8	27.0
(^{ipr}PCOP)Ir	−8.5	36.1	7.7	23.6	−24.6	0.4	20.7	16.1	−15.8	7.9	25.4	2.3	−21.8	30.8

2.2. Comparison between the Two Ligands ^{ipr}PCP and ^{ipr}PCOP

The differences in δE between the (^{ipr}PCP)Ir-catalyzed reaction and the (^{ipr}PCOP)Ir-catalyzed process are well within the margin of error for the three pathways ($\Delta\delta E^{pathA}$ = 1.5 kcal mol^{-1}, $\Delta\delta E^{pathB}$ = 1.8 kcal mol^{-1} and $\Delta\delta E^{pathC}$ = 3.8 kcal mol^{-1}). Similar to the (^{ipr}PCP)Ir-catalyzed reaction, the observed trend in δE for the reaction along all three pathways is path B > path C > path A. Thus, there is also a kinetic preference for the pathway which begins with the C-H addition for the (^{ipr}PCOP)Ir-catalyzed β-O-4 compound in lignin.

2.3. The Reaction of (^{ipr}PCP)Co with 2-Phenoxy-1-phenylehtanol

Figures 7–12 show the optimized geometries as well as the Gibbs free energy profiles for the catalytic dehydroaryloxylation of 2-phenoxy-*1*-phenylehtanol **1** using (^{ipr}PCP)Co along pathways A, B and C, respectively. All stationary points have been sought on both

the singlet and triplet potential energy surface as shown in Tables 7–9, with the triplet state reactants being 77.2 kcal mol^{-1} less stable than the singlet state reactants. Along pathway A, the (^{ipr}PCP)Co-catalyzed cleavage of **1** proceeds initially via C-H addition through **TSA1** with an activation barrier of 13.9 kcal mol^{-1} to form **A2**, whereas C-O bond insertion follows via **TSA2** with an activation barrier of 17.9 kcal mol^{-1}. The abstracted hydrogen sits axially to the aromatic backbone of the pincer ligand in **TSA1** but shifts to an equatorial position during the C-O bond cleavage, while the cleaved phenolate replaces it in the axial position in **TSA2**. It is found that the six-membered intermediate is not formed after the C-O bond cleavage occurs, as the enolate is released in this step with a reaction energy of 27.9 kcal mol^{-1} to form **A3**, containing only the phenoxide and the hydrogen ligand. The transition states for the C-H addition and C-O insertion, as well as the intermediate **A2**, were found not to exist on the triplet surface. Finally, reductive elimination of phenol **5** proceeds via **TSA3** with an activation barrier of 26.3 kcal mol^{-1} leading to the regeneration of the catalyst. The formation of **A3+[6+7]** at −22.4 kcal mol^{-1} is the major resting state in the catalytic cycle, being only lower than the final products **CoPCP +[5+7]** by 0.6 kcal mol^{-1}. On the triplet surface, the formation of **A3** is endergonic by 24.1 kcal mol^{-1}, making it less stable than the singlet state **A3** by 46.5 kcal mol^{-1}. These energies show that the major product formed from the ^{ipr}PCPCo-catalyzed cleavage of a lignin β-O-4 compound is acetophenone and a two-state reactivity was not observed in the catalytic cycle.

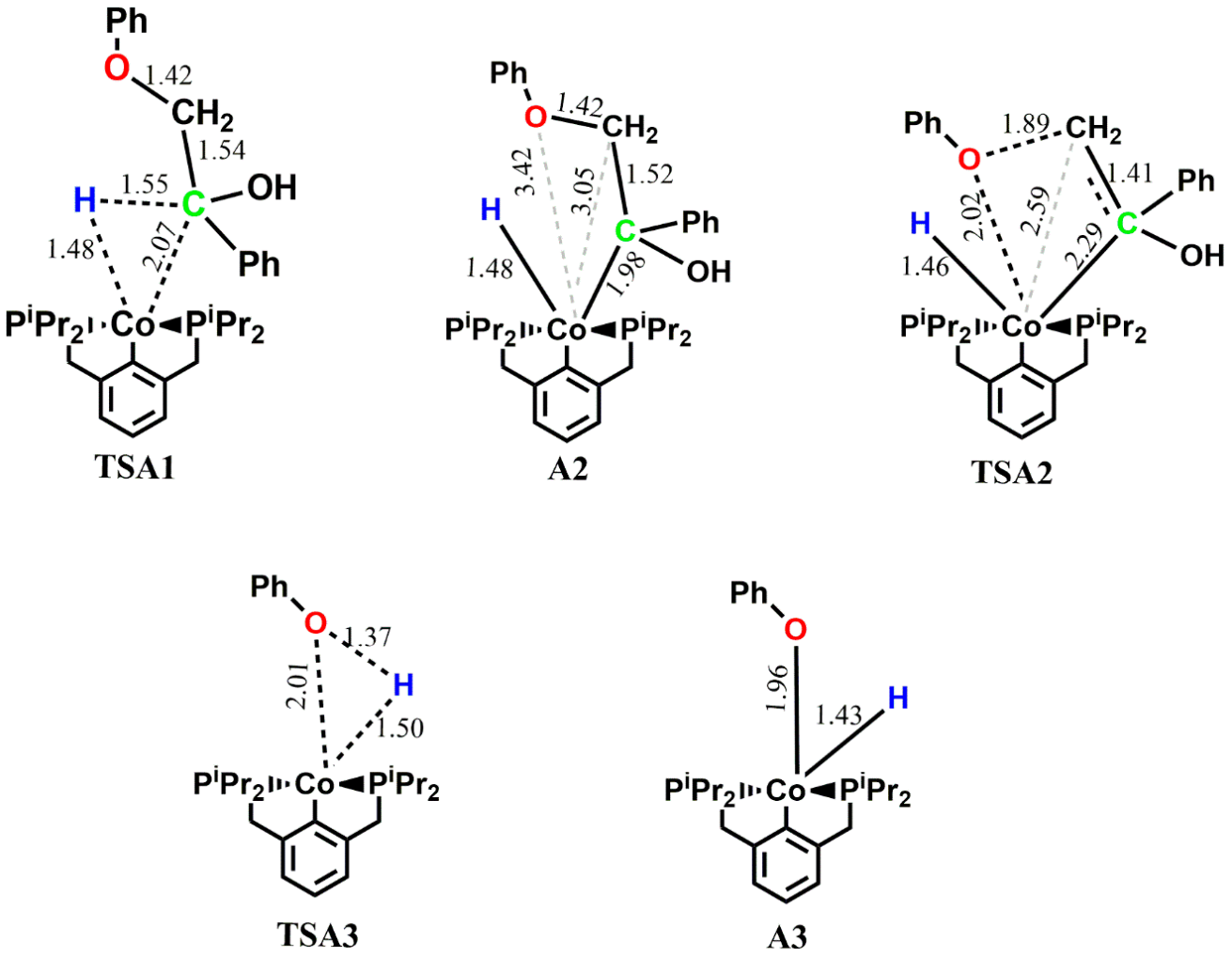

Figure 7. Optimized geometries of the main stationary points involved in the reaction of **(^{ipr}PCP)Co** with 2-phenoxy-1-phenylethanol **1** along pathway A. Distances in Å.

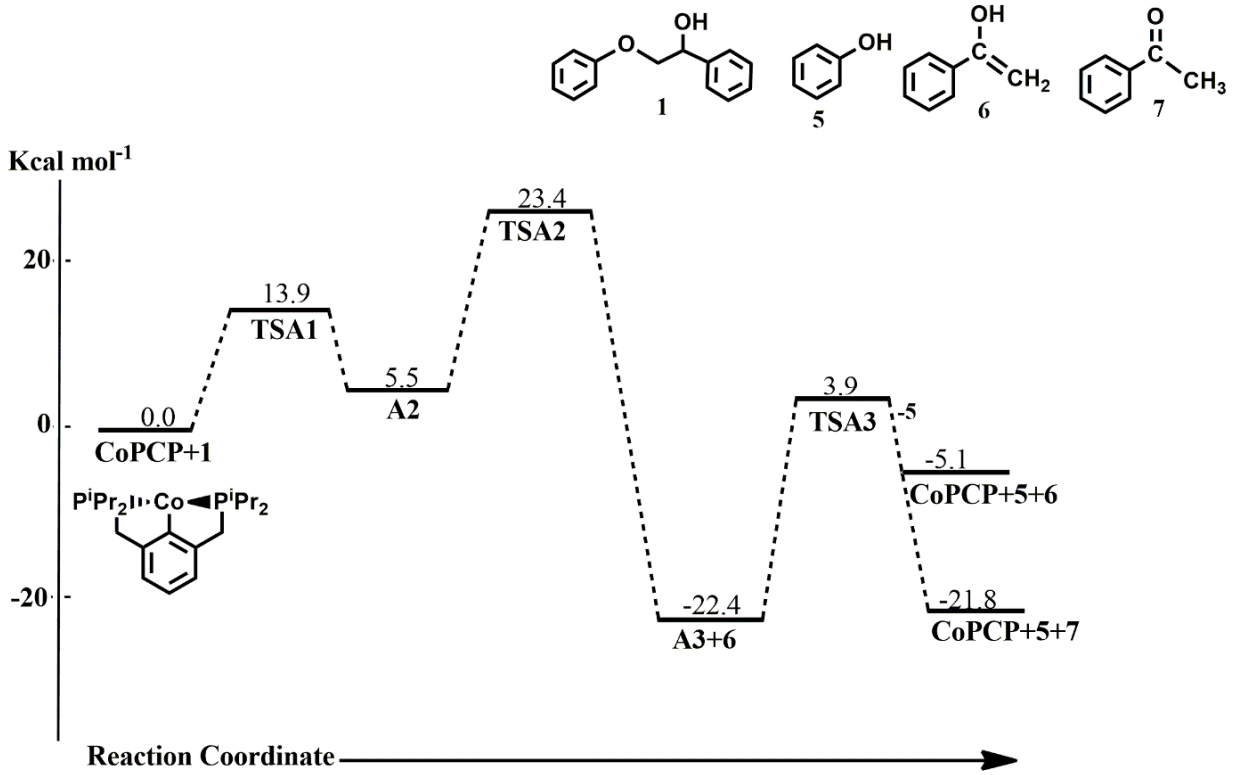

Figure 8. Free energy landscape for the overall catalytic cycle for the reaction of (^{ipr}PCP)Co with **1** along pathway A.

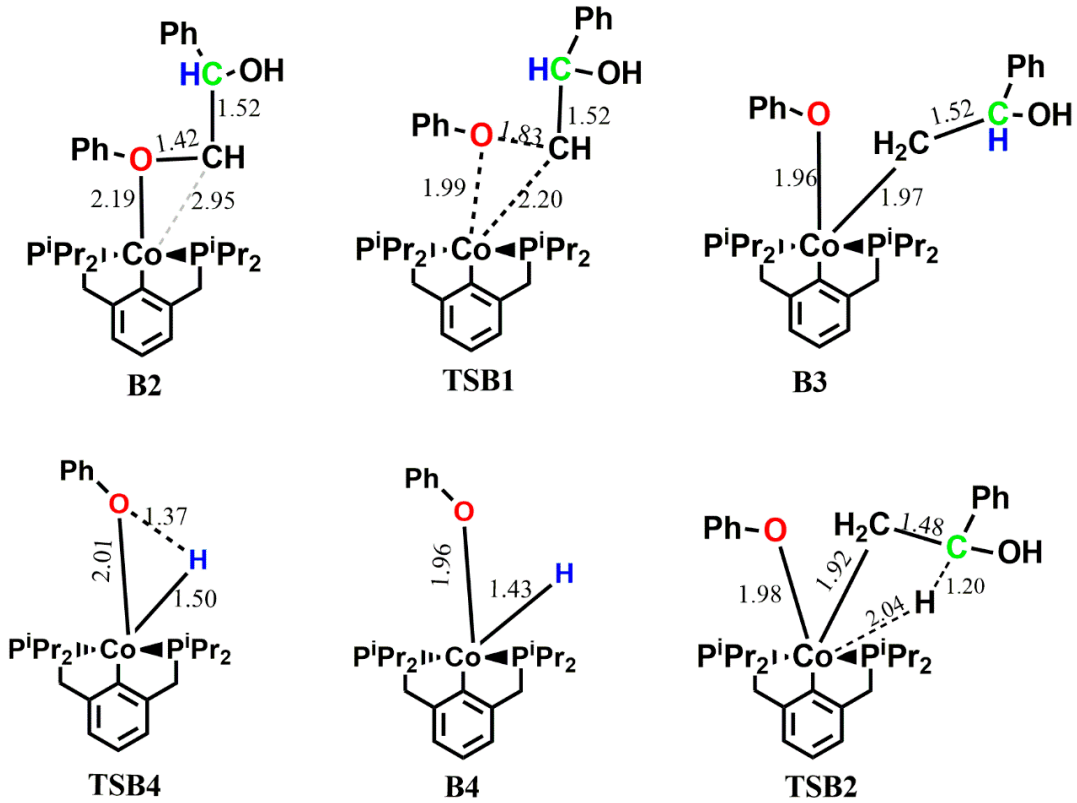

Figure 9. Optimized geometries of the main stationary points involved in the reaction of (^{ipr}PCP)Co with 2-phenoxy-*1*-phenylethanol **1** along pathway B. Distances in Å.

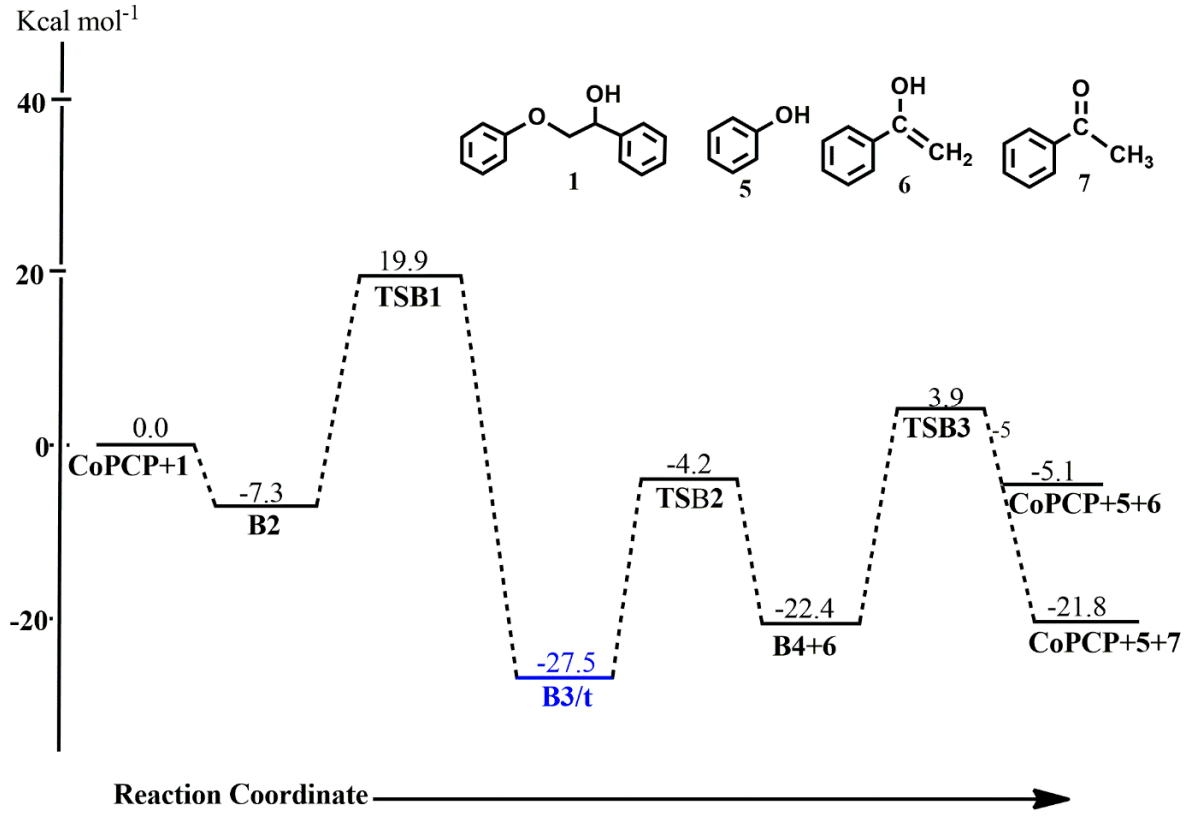

Figure 10. Free energy landscape for the overall catalytic cycle for the reaction of (*ipr*PCP)Co with **1** along pathway B. Triplet state energies shown in blue.

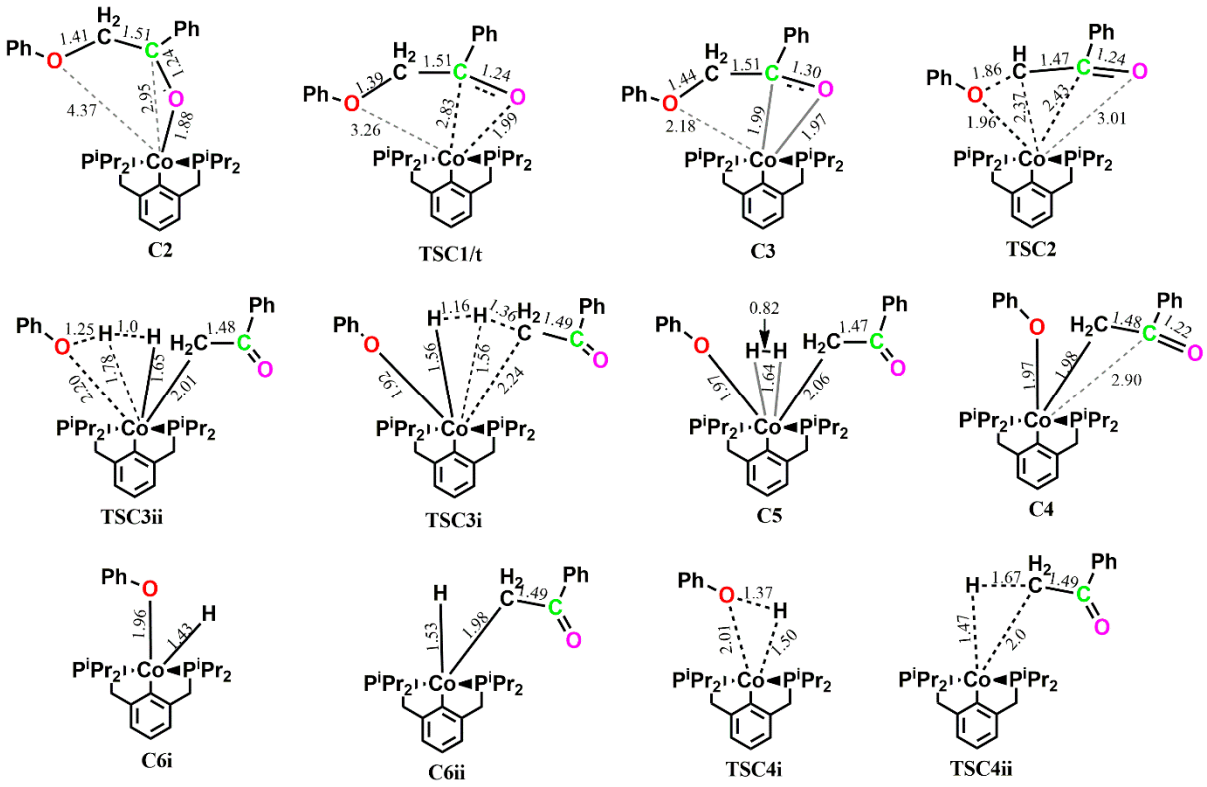

Figure 11. Optimized geometries of the main stationary points involved in the reaction of (*ipr*PCP)Co with 2-phenoxy-*1*-phenylethanol **1** along pathway C. Distances in Å.

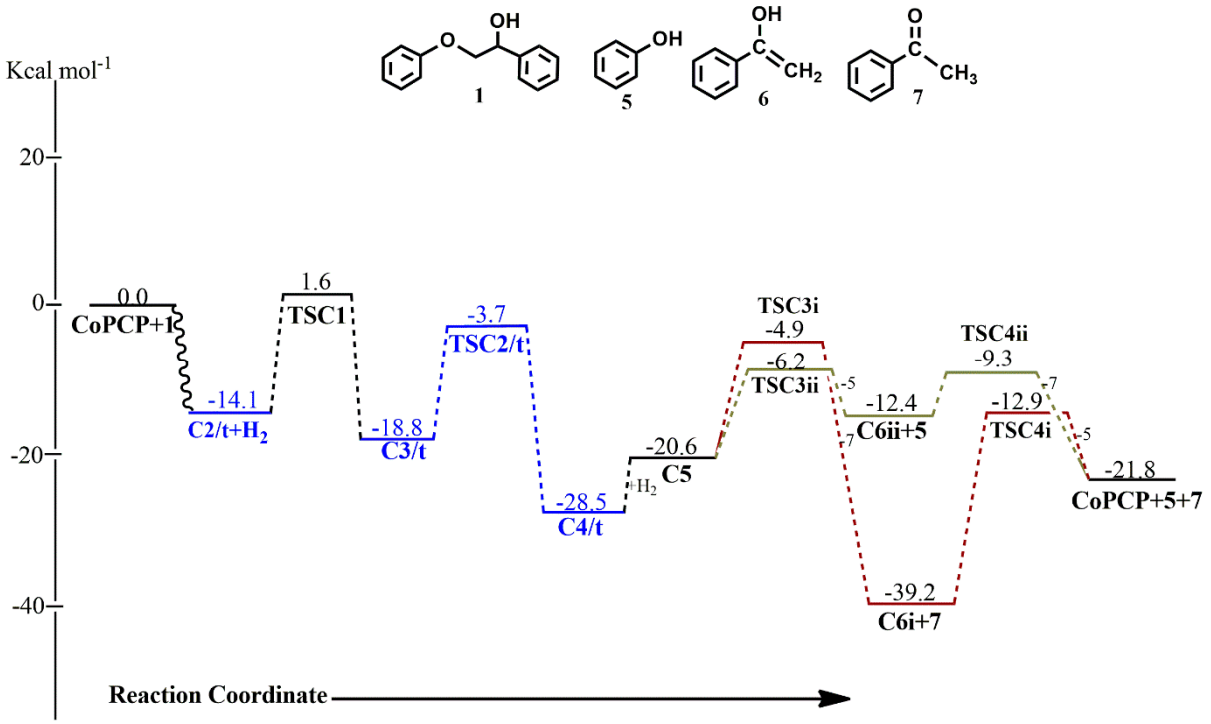

Figure 12. Free energy landscape for the overall catalytic cycle for the reaction of **(^{ipr}PCP)Co** with **1** along pathway C. Triplet state energies shown in blue.

Table 7. Comparison of singlet-state and triplet-state energies of the stationary points involved in the reaction of **(^{ipr}PCP)Co** with **1** along pathway A.

	Singlet State/Kcal mol^{-1}	**Triplet State/Kcal mol^{-1}**
CoPCP+1	0.0	77.2
TSA1	13.9	Could not be located
A2	5.5	Could not be located
TSA2	23.4	Could not be located
A3+6+7	−22.4	24.1
TSA3	3.9	53.6
CoPCP+5+6	−5.1	136.8
CoPCP+5+7	−21.8	138.9

Table 8. Comparison of singlet-state and triplet-state energies of the stationary points involved in the reaction of **(^{ipr}PCP)Co** with **1** along pathway B.

	Singlet State/Kcal mol^{-1}	**Triplet State/Kcal mol^{-1}**
CoPCP+1	0.0	77.2
B2	−7.3	Could not be located
TSB1	19.9	Could not be located
B3	−17.7	−27.5
TSB2	−4.2	Could not be located
B4+6+7	−22.4	24.1
TSB3	3.9	53.6
CoPCP+5+6	−5.1	136.8
CoPCP+5+7	−21.8	138.9

Table 9. Comparison of singlet-state and triplet-state energies of the stationary points involved in the reaction of **(*ipr*PCP)Co** with **1** along pathway C.

	Singlet State/Kcal mol^{-1}	Triplet State/Kcal mol^{-1}
CoPCP+1	0.0	77.2
C2	−9.9	−14.1
TSC1	1.6	Could not be located
C3	−17.9	−18.8
TSC2	15.3	−3.7
C4	−24.3	−28.5
C5	−20.6	−10.3
TSC3i	−4.9	1.6
TSC3ii	−6.2	−3.7
C6i+7	−39.2	69.3
C6ii+5	−12.4	26.3
TSC4i	−12.9	83.2
TSC4ii	−9.3	55.8
CoPCP+5+7	−21.8	138.9

In the (*ipr*PCP)Co-catalyzed reaction of **1** along pathway B, the ether oxygen forms a covalent bond with the cobalt complex to give an adduct **B2** in an exergonic reaction (ΔG° = −7.3 kcal mol^{-1}). Direct ether cleavage via C-O bond addition follows with an activation energy barrier of 27.2 kcal mol^{-1}, leading to the O-bound and C-bound complex **B3**. Here, a two-state reactivity is observed, as the triplet state **B3** is found to be more stable than the singlet state **B3** by 9.8 kcal mol^{-1}. The ether-carbon transitions from a position axial to the aromatic backbone in **TSB1** to an equatorial position in **B3**, while the ether-oxygen sits axially to the aromatic backbone in both **TSB1** and **B3**. Subsequent hydrogen abstraction via C-H addition to the metal center proceeds from the more stable triplet-state **B3/t** via singlet-state **TSB2** with an activation energy barrier of 23.3 kcal mol^{-1} to form a singlet-state **B4** which is endergonic by 5.1 kcal mol^{-1}. Similar to pathway A, cleavage of the enolate occurs in this step leaving only the phenolate and the hydride bound to the metal center, as seen in intermediate **B4** which then undergoes reductive elimination of the phenol and regeneration of the catalyst with an activation energy barrier of 26.3 kcal mol^{-1}. The enolate **6**, and the more stable acetophenone **7**, to which it rearranges, are also shown to be the major products formed in this reaction. Apart from the intermediate **B3**, all other stationary points along the reaction cycle are found to be unstable on the triplet PES.

In the (*ipr*PCP)Co-catalyzed reaction of **1** along pathway C, all but one of the stationary points in the catalytic cycle exhibit multiple spin ground states, where more than one of those stationary points with lower energies belong to the higher spin state and a two-state reactivity is observed as shown in Figure 12. The coordination of the ketone substrate to the metal center to form the adduct **C2** is exergonic by −14.1 kcal mol^{-1} on the triplet surface and −9.9 kcal mol^{-1} on the singlet surface. This causes subsequent rearrangement of the adduct to form **C3** containing the η^2-bound ketone to proceed via **TSC1** with an activation energy barrier of 15.7 kcal mol^{-1} instead of a lower barrier of 11.5 kcal mol^{-1}. Similar to what was observed in the (*ipr*PCP)Ir-catalyzed reaction, the ketone-carbon transitions from having no significant interaction with the cobalt center in C2 ($d_{\text{Ir-C}}$ = 2.95 Å) to forming a covalent bond with the metal center in **C3** ($d_{\text{Ir-C}}$ = 1.99 Å), and moves from occupying an axial position relative to the aromatic backbone of the pincer ligand in **C2** to an equatorial position in **C3**. The bond distance between the ether-oxygen and the metal center also reduces from 4.37 Å to 2.18 Å after the rearrangement of **C2** to **C3**, bringing the ether oxygen in close proximity for subsequent C-O bond cleavage. Ether bond cleavage via **TSC2/t** is kinetically more favored on the triplet surface with an activation energy barrier of 15.1 kcal mol^{-1} ($Ea^{[\text{singlet state}]}$ = 33.2 kcal mol^{-1}), leading to the formation of

the triplet state O-bound and C-bound ketone **C4/t**, which is exergonic by 28.5 kcal mol^{-1} and more stable than the singlet-state **C4** by 4.2 kcal mol^{-1}. The phenolate occupies the axial position relative to the aromatic backbone of the pincer ligand, while the ketone occupies the equatorial position. However, both the phenolate and the ketone move equatorially to the pincer ligand after hydrogenation occurs, putting the η^2–H_2 in the axial position in **C5**. The hydrogenation step is endergonic by 18.2 kcal mol^{-1} on the triplet surface and endergonic by 3.7 kcal mol^{-1} on the singlet surface. Similar to the observed trend in the (^{ipr}PCP)Ir-catalyzed reaction, the phenol is the kinetic product while the acetophenone is the thermodynamic product. Reductive elimination of the phenol first proceeds with an activation barrier of 14.4 kcal mol^{-1} with the released product being formed at −12.4 kcal mol^{-1}, while initial release of the acetophenone proceeds with activation barrier of 15.7 kcal mol^{-1} and the released product is formed at −39.2 kcal mol^{-1}. The intermediate **C5**, and the transition states **TSC3i** and **TSC3ii** are all found to be more stable on the singlet surface. Subsequent release of the acetophenone from **C6ii**, which proceeds with an activation energy barrier of 3.1 kcal mol^{-1} on the singlet surface, and is lower than the triplet state activation energy barrier by 26.4 kcal mol^{-1}, leads to the release of the catalyst, which is exergonic by 9.4 kcal mol^{-1}, while subsequent release of the phenol from **C6i** proceeds with an activation energy barrier of 26.3 kcal mol^{-1} which is less kinetically favored for the release of the catalyst. Hence, the likely observed product from this sequence of product release would be **C6i+7**.

Tables 10–12 show the comparison in activation energies, energies of formation and apparent activation energies (δE) for the entire cycles, calculated for the three pathways and two different ligand combinations. The trend observed here in the activation energies and apparent activation energies (δE) for the entire cycle is different from the (^{ipr}PCP)Ir-catalyzed process. The activation barrier for the C-O bond addition is seen to be lower in pathway C (Ea = 15.1 kcal mol^{-1}) than pathways A (Ea = 17.9 kcal mol^{-1}) and B (Ea = 27.2 kcal mol^{-1}), whereas, ultimately, the calculated apparent activation energies (δE) for pathway C are shown to be kinetically favored by 15.7 kcal mol^{-1} over pathway A and by 17.3 kcal mol^{-1} over pathway B. These energetics show that the kinetically favored pathway for the (^{ipr}PCP)Co-catalyzed cleavage of a β-O-4 compound is pathway C, which involves the ketone motif of the substrate and begins with the C-O bond addition, even when the desired product is acetophenone (δE = 16.7 kcal mol^{-1}).

Table 10. Activation energies and reaction energies for the reaction of **1** with **[CoPCP]** and **[CoPOCP]** along pathway A. Energies in kcal mol^{-1}.

	EaA1	**ΔEA2**	**EaA2**	**ΔEA3**	**EaA3**	**Δ*Gr***	**δE**
(^{ipr}PCP)Co	13.9	5.5	17.9	−27.9	26.3	−21.8	24.0
(^{ipr}PCOP)Co	9.7	5.1	19.4	−28.5	22.3	−21.8	26.1

Table 11. Activation energies and reaction energies for the reaction of **1** with **[CoPCP]** and **[CoPOCP]** along pathway B. Energies in kcal mol^{-1}.

	ΔEB2	**EaB1**	**ΔEB3**	**EaB2**	**ΔEB4**	**EaB4**	**Δ*Gr***	**δE**
(^{ipr}PCP)Co	−7.3	27.2	−10.4	13.5	−4.7	26.3	−21.8	25.6
(^{ipr}PCOP)Co	−10.6	34.2	−7.3	14.2	−5.4	22.3	−21.8	28.6

Table 12. Activation energies and reaction energies for the reaction of **1** with **[CoPCP]** and **[CoPOCP]** along pathway C. Energies in kcal mol^{-1}.

	ΔEC2	**EaC1**	**ΔEC3**	**EaC2**	**ΔEC4**	**ΔEC5**	**EaC3i**	**EaC3ii**	**ΔEC6i+7**	**ΔEC6ii+5**	**EaC4i**	**EaC4ii**	**Δ*Gr***	**δE**
(^{ipr}PCP)Co	−14.1	15.8	−4.6	15.1	−28.5	−20.6	15.7	14.4	−18.6	8.2	26.3	3.1	−21.8	8.3
(^{ipr}PCOP)Co	−16.2	6.4	0.5	11.8	−14.8	13.8	13.1	13.1	−23.4	−4.0	22.3	7.9	−21.8	2.8

2.4. (^{ipr}PCP) vs. (^{ipr}PCOP)

The differences in the apparent activation energy (δE) between the (^{ipr}PCP)Co-catalyzed process and the (^{ipr}PCOP)Co-catalyzed process are also well within the margin of error for all three pathways ($\Delta\delta E^{pathA}$ = 2.1 kcal mol^{-1}, $\Delta\delta E^{pathB}$ = 3.0 kcal mol^{-1}, $\Delta\delta E^{pathC}$ = 5.5 kcal mol^{-1}). When we compare the δE values for the (^{ipr}PCOP)Co-catalyzed reaction among all three pathways, the observed trend is path B > path A > path C. These values also show that pathway C is the kinetically favored pathway for the (^{ipr}PCOP)Co-catalyzed cleavage of the β-O-4 linkage in lignin, and that the PCOP ligand displays comparatively similar catalytic activity to the PCP ligand.

2.5. Iridium vs. Cobalt

Along pathway A, the (^{ipr}PCP)Ir-catalyzed process is kinetically favored by 8.8 kcal mol^{-1} over the (^{ipr}PCP)Co-catalyzed reaction, while along pathways B and C, the Co-catalyzed reaction is kinetically favored over their Ir-catalyzed counterpart by 6.4 kcal mol^{-1} and 18.7 kcal mol^{-1}, respectively. From the obtained data, the use of the (^{ipr}PCP)Co catalyst for the cleavage of alkyl aryl ethers is a comparable alternative to the (^{ipr}PCP)Ir catalyst, with the Co being more active, although the (^{ipr}PCP)Co-catalyzed process reaction would preferably proceed via direct C-O insertion, while the (^{ipr}PCP)Ir-catalyzed process would rather proceed via direct C-H addition.

2.6. Calculation of Rate Constants for the Cleavage Reactions

The apparent activation energies are used to calculate the rate constants of the reactions using the equation derived from Erying's transition state theory [21], where ΔG° in the equation is replaced by δE.

$$k(T) = \frac{K_B T}{h} e^{\frac{-\delta E}{RT}} \quad (1)$$

The rate constant k(T) is also defined as the turnover frequency (TOF) by Kozuch and Shaik [22] based on the energetic span approximation. Taking the temperature as 298.15 K, the computed rate constants/TOF are shown in Table 13 below.

Table 13. Rate constants for the (^{ipr}PCP)Ir-and (^{ipr}PCP)Co-catalyzed cleavage of the lignin β-O-4 linkage along all three pathways. T = 298.15 K.

	Path A/s^{-1}	**Path B/s^{-1}**	**Path C/s^{-1}**
(^{ipr}PCP)Ir	44.7	2.2×10^{-11}	1.0×10^{-7}
(^{ipr}PCP)Co	1.6×10^{-5}	1.1×10^{-6}	5.1×10^{6}

It is apparent from these rate constant values that the fastest reaction is the cleavage of the β-O-4 linkage with the (^{ipr}PCP)Co catalyst via the pathway which involves the ketone motif of the substrate and proceeds via direct C-O bond insertion (Path C), followed by the use of the (^{ipr}PCP)Ir catalyst via the direct C-H bond addition mechanism (Path A). The fact that more intermediates and transition states occur in the triplet state along pathway C for the cleavage reaction using (^{ipr}PCP)Co greatly affects the kinetics of the reaction, causing it to proceed much faster.

3. Computational Details

All calculations were carried out using the Spartan 14 Molecular Modelling program [23] and the Gaussian 09 package [24]. The structures and energies of all the stationary points along the reaction pathways were computed using the M06 functional. The reference energy and the energy differences for each stationary point in the "free energy landscape" figures correspond to the reactants; these are the Ir/Co catalyst and 2-phenoxy-*1*-phenylethanol (I). The atoms hydrogen and argon were described with the 6-311G** basis set [25], while the metals Ir and Co were modeled with the quasi-relativistic

pseudopotential of triple-ζ quality, LANL2TZ [26,27]. The M06 functional is a hybrid meta-gradient-corrected functional (meta-GGA) with 27% of Hartree–Fock exchange, which has been benchmarked and is recommended for the study of organometallic thermochemistry as well as non-covalent interactions [28,29]. All stationary points were verified by full frequency calculations. Minima (reactants, intermediates and products) were shown to have a Hessian matrix whose eigenvalues are all positive, leading to vibrational frequencies that are real, while transition states were shown to have a Hessian matrix with all positive eigenvalues, except for a single negative eigenvalue characterized by a vibration along the reaction coordinate.

The starting geometries of the molecular systems were constructed using Spartan's graphical model builder and minimized interactively using the sybyl force field. Input structures for transition state (TS) optimizations were obtained after a potential energy surface (PES) scan was performed for each reaction step. This calculation was also useful in showing that the minima obtained do in fact correspond to the reactant and product for that step. The PES scan gives an approximate transition state structure, which is then submitted for transition state calculations using the synchronous Transit-Guided Quasi-Newton (STQN) Method developed by Schlegel and coworkers [30]. General effects of a surrounding solvent were evaluated using a polarizable continuum model derived with an integral equation formalism (IEF-PCM) [31] of *p*-xylene solvation, which is the solvent used in experiments. However, the calculations that included solvent effects showed differences of just <2 kcal/mol in the calculated barrier heights with gas phase calculations, and hence only gas phase calculations are reported below.

The apparent activatis.n energy, also known as the rate-limiting activation energy, of the catalytic cycle is obtained from the energetic span model as defined by Kozuch and Shaik [22], which is an extension of the Curtin–Hammett principle. Two terms appear in this model that determine the turnover frequency (TOF) of a catalytic cycle: the TDTS (TOF-determining transition state) and the TDI (TOF-determining intermediate). These species define the energetic span within the cyclic constraints and in turn measure the kinetics of the catalytic cycle. The energetic span, δE, is thus defined as

$$\delta E = \begin{cases} T_{TDTS} - T_{TDI} & \text{if TDTS appears after TDI} \\ T_{TDTS} - T_{TDI} + \Delta G_r & \text{if TDTS appears before TDI} \end{cases} \quad (2)$$

To ascertain the suitability of the M06 functional to give reliable energetics, some of the steps of the cycle were computed at the M06-2X-D3 level for comparison. The M06-2X-D3 optimized geometries are very similar to those of the M06 geometries, and the differences in activation barriers range from 0 to 5 kcal mol^{-1} (Supporting Information, Tables S1–S3).

4. Conclusions

We have reported the kinetics and thermodynamics of the cleavage of a model of the β-O-4 linkage in lignin (*2*-phenoxy-*1*-phenylethanol) using iridium and cobalt pincer complexes. The observed selectivity for the initial C-H addition mechanism (Path A) for the cleavage reaction in experiment [11,13] is confirmed, as the initial C-H addition pathway is kinetically favored by 16.8 kcal mol^{-1} over the direct C-O insertion pathway in the (^{ipr}PCP)Ir-catalyzed reaction.

The cobalt catalysts show a kinetic preference for the mechanism that involves an initial dehydrogenative equilibrium of the substrate with its ketone motif, and then proceeds via direct C-O insertion (Path C). This pathway is found to be kinetically favored by 15.7 kcal mol^{-1} over the initial C-H addition pathway.

The cleavage reaction is kinetically controlled, having a rate constant of 44.7 s^{-1} when the (^{ipr}PCP)Ir catalyst is used and a rate constant of 5.1 × 10^6 s^{-1} when the (^{ipr}PCP)Co is used. The cobalt-pincer catalyst has been shown to be more active for the cleavage reaction, having a two-state reactivity along the catalytic cycle, which greatly reduces its activation barrier.

It is observed from the calculated energies that the kinetic product is the phenol, while the acetophenone is the thermodynamic product for both the iridium- and cobalt-catalyzed reactions. The catalyst can be recovered easily when cobalt is used and when the phenol is the desired product.

Some of the intermediates and the transition states located in this work display multiple-spin ground states and a two-state reactivity is observed in the (^{ipr}PCP)Co-catalyzed reaction.

In summary, this study has shown that PCP-type iridium and cobalt catalysts are active towards the cleavage of alkyl aryl ethers, such as the β-O-4 linkage in lignin, and it has provided molecular level insights into the preferred mechanism for the cleavage reactions. This new knowledge will aid in the design of an atom-economic catalyst for the cleavage of alkyl aryl ethers, which are widely used in chemistry, as well as the valorization of lignin towards the production of value-added aromatic compounds.

Supplementary Materials: The following supporting information can be downloaded at https://www.mdpi.com/article/10.3390/catal13040757/s1, Table S1: Comparison between the M06 and M06-2X-D3 levels of theories calculated relative energies, activation energies and energies of formation for the IrPCP catalyzed cleavage of 2-Phenoxy-*1*-phenylethanol along Pathway A; Table S2: Comparison between the M06 and M06-2X-D3 levels of theories calculated relative energies, activation energies and energies of formation for the IrPCP catalyzed cleavage of *2*-Phenoxy-*1*-phenylethanol along Pathway B; Table S3: Comparison between the M06 and M06-2X-D3 levels of theories calculated relative energies, activation energies and energies of formation for the IrPCP catalyzed cleavage of *2*-Phenoxy-*1*-phenylethanol along Pathway C; S4: XYZ coordinates of the optimized structures.

Author Contributions: R.T., E.A. and N.H.d.L. conceived the study. M.M. carried out the study. M.M., R.T. and E.A. analyzed the results. M.M., R.T., E.A. and N.H.d.L. wrote the paper. All authors have read and agreed to the published version of the manuscript.

Funding: This research was funded by UK Department of International Development via the Royal Society (grant reference AQ140028) under the Africa Capacity Building Initiative, and Teaching and Learning Innovation Fund (TALIF) of the National Council for Tertiary Education, Ghana, grant number [KNUSTR/3/008/2005]

Data Availability Statement: The original contributions presented in the study are included in the article/Supplementary Material, and further inquiries can be directed to the corresponding author.

Acknowledgments: The authors acknowledge the Royal Society and the UK Department for International Development for a research grant under the Africa Capacity Building Initiative (ACBI), which has funded this research. We also acknowledge the Centre for High Performance Computing, South Africa, for access to additional computing facilities. M.M., R.T. and E.A. are also grateful to the National Council for Tertiary Education, Ghana, for a Teaching and Learning Innovation Fund (TALIF) grant.

Conflicts of Interest: The authors declare that they have no conflict of interest regarding this manuscript. We declare that the funding source had no influence on the study design; on the collection, analysis and interpretation of data; or on the writing of this manuscript.

References

1. Mancano, G.; Page, M.J.; Bhadbhade, M.; Messerle, B.A. Hemilabile and bimetallic coordination in Rh and Ir complexes of NCN pincer ligands. *Inorg. Chem.* **2014**, *53*, 10159–10170. [CrossRef]
2. Gupta, M.; Hagen, C.; Flesher, R.J.; Kaska, W.C.; Jensen, C.M. A highly active alkane dehydrogenation catalyst: Stabilization of dihydrido rhodium and iridium complexes by a P-C-P pincer ligand. *Chem. Comm.* **1996**, *17*, 2083–2084. [CrossRef]
3. Kanzelberger, M.; Singh, B.; Czerw, M.; Krogh-Jespersen, K.; Goldman, A.S. Addition of C-H bonds to the catalytically active complex (PCP)Ir (PCP = η3-2,6-((t)Bu2PCH2)2C6H3). *J. Am. Chem. Soc.* **2000**, *122*, 11017–11018. [CrossRef]
4. Lui, F.; Pak, E.B.; Singh, B.; Jensen, C.M.; Goldman, A.S. Dehydrogenation of n-Alkanes Catalyzed by Iridium "Pincer" Complexes: Regioselective Formation of α-Olefins. *J. Am. Chem. Soc.* **1999**, *121*, 4086–4087.
5. Trovitch, R.J.; Lobkovsky, E.; Bouwkamp, M.W.; Chirik, P.J. Carbon-oxygen bond cleavage by bis(imino)pyridine iron compounds: Catalyst deactivation pathways and observation of acyl C-O bond cleavage in esters. *Organometallics* **2008**, *27*, 6264–6278. [CrossRef]

6. Conejero, S.; Paneque, M.; Poveda, M.L.; Santos, L.L.; Carmona, E. C-H bond activation reactions of ethers that generate iridium carbenes. *Acc. Chem. Res.* **2010**, *43*, 572–580. [CrossRef] [PubMed]
7. Santos, L.L.; Mereiter, K.; Paneque, M. Reaction of 2-methylanisole with TpMe2Ir(C6H 5)2(N2): A comprehensive set of activations. *Organometallics* **2013**, *32*, 565–569. [CrossRef]
8. Lara, P.; Paneque, M.; Poveda, M.L.; Salazar, V.; Santos, L.L. Formation and cleavage of C-H, C-C, and C-O bonds of ortho-methyl-substituted anisoles by late transition metals. *J. Am. Chem. Soc.* **2006**, *128*, 3512–3513. [CrossRef] [PubMed]
9. Whited, M.T.; Zhu, Y.; Timpa, S.D.; Chen, C.H.; Foxman, B.M.; Ozerov, O.V.; Grubbs, R.H. Probing the C-H activation of linear and cyclic ethers at (PNP)Ir. *Organometallics* **2009**, *28*, 4560–4570. [CrossRef]
10. Kundu, S.; Choi, J.; Wang, D.Y.; Choliy, Y.; Emge, T.J.; Krogh-Jespersen, K.; Goldman Alan, S. Cleavage of ether, ester, and tosylate C(sp3)-O bonds by an iridium complex, initiated by oxidative addition of C-H bonds. Experimental and computational studies. *J. Am. Chem. Soc.* **2013**, *135*, 5127–5143. [CrossRef]
11. Zakzeski, J.; Bruijnincx, P.C.A.; Jongerius, A.L.; Weckhuysen, B.M. The Catalytic Valorization of Ligning for the Production of Renewable Chemicals. *Chem. Rev.* **2010**, *110*, 3552–3599. [CrossRef] [PubMed]
12. Haibach, M.C.; Lease, N.; Goldman, A.S. Catalytic cleavage of ether C-O bonds by pincer iridium complexes. *Angew. Chem.-Int. Ed.* **2014**, *53*, 10160–10163. [CrossRef]
13. Nichols, J.M.; Bishop, L.M.; Bergman, R.G.; Ellman, J.A. Catalytic C-O bond cleavage of 2-aryloxy-1-arylethanols and its application to the depolymerization of lignin-related polymers. *J. Am. Chem. Soc.* **2010**, *132*, 12554–12555. [CrossRef] [PubMed]
14. Haibach, M.C.; Guan, C.; Wang, D.Y.; Li, B.; Lease, N.; Steffens, A.M.; Krogh-Jespersen, K.; Goldman, A.S. Olefin hydroaryloxylation catalyzed by pincer-iridium complexes. *J. Am. Chem. Soc.* **2013**, *135*, 15062–15070. [CrossRef]
15. Ueno, S.; Mizushima, E.; Chatani, N.; Kakiuchi, F. Direct observation of the oxidative addition of the aryl carbon-oxygen bond to a ruthenium complex and consideration of the relative reactivity between aryl carbon-oxygen and aryl carbon-hydrogen bonds. *J. Am. Chem. Soc.* **2006**, *128*, 16516–16517. [CrossRef]
16. Chmely, S.; Kim, S.; Paton, R.; Beckham, G.; Ciesielski, P.; Jiménez-Osés, G. Mechanistic study of a Ru-xantphos catalyst for tandem alcohol dehydrogenation and reductive aryl-ether cleavage. *ACS Catal.* **2013**, *3*, 963–974. [CrossRef]
17. Liu, C.; Wilson, A.K. Cleavage of the βo4 linkage of lignin using group 8 pincer complexes: A DFT study. *J. Mol. Catal. A Chem.* **2015**, *399*, 33–41. [CrossRef]
18. Junge, K.; Papa, V.; Beller, M. Cobalt–Pincer Complexes in Catalysis. *Chem. Eur. J.* **2019**, *25*, 122–143. [CrossRef]
19. Wu, A.; Patrick, B.O.; Chung, E.; James, B.R. Hydrogenolysis of β-O-4 lignin model dimers by a ruthenium-xantphos catalyst. *Dalt. Trans.* **2012**, *41*, 11093. [CrossRef]
20. Kim, S.; Chmely, M.; Nimlos, S.; Bomble, Y.; Foust, T.; Beckham, G. Computational Study of Bond Dissociation Enthalpies for a Large Range of Native and Modified Lignins. *J. Phys. Chem. Lett.* **2011**, *2*, 2846–2852. [CrossRef]
21. Erying, H. The Activated Complex in Chemical Reactions. *J. Chem. Phys.* **1935**, *3*, 107. [CrossRef]
22. Kozuch, S.; Shaik, S. How to conceptualize catalytic cycles? The energetic Span model. *Acc. Chem. Res.* **2011**, *44*, 101–110. [CrossRef] [PubMed]
23. Spartan, Wavefunction, Inc.: Irvine, CA, USA. Available online: https://www.wavefun.com/spartan (accessed on 1 March 2023).
24. Frisch, M.J.; Trucks, G.W.; Schlegel, H.B.; Scuseria, G.E.; Robb, M.A.; Cheeseman, J.R.; Scalmani, G.; Barone, V.; Petersson, G.A.; Nakatsuji, H.; et al. *Gaussian 09 (Revision A. 02) [Computer Software]*, Gaussain Inc.: Wallington, CT, USA, 2009.
25. Rassolov, V.A.; Pople, J.A.; Ratner, M.A.; Windus, T.L. 6-31G* basis set for atoms K through Zn. *J. Chem. Phys.* **1998**, *109*, 1223–1229. [CrossRef]
26. Hay, P.J.; Wadt, W.R. A b initio effective core potentials for molecular calculations. Potentials for the transition metal atoms Sc to Hg. *J. Chem. Phys.* **1985**, *82*, 270–283. [CrossRef]
27. Wadt, W.R.; Hay, P.J. Ab initio effective core potentials for molecular calculations. Potentials for main group elements Na to Bi. *J. Chem. Phys.* **1985**, *82*, 284–298. [CrossRef]
28. Zhao, Y.; Truhlar, D.G. The M06 suite of density functionals for main group thermochemistry, thermochemical kinetics, noncovalent interactions, excited states, and transition elements: Two new functionals and systematic testing of four M06-class functionals and 12 other function. *Theor. Chem. Acc.* **2008**, *120*, 215–241. [CrossRef]
29. Liu, C.; Peterson, C.; Wilson, A.K. C-O bond cleavage of dimethyl ether by transition metal ions: A systematic study on catalytic properties of metals and performance of DFT functionals. *J. Phys. Chem. A* **2013**, *117*, 5140–5148. [CrossRef]
30. Peng, C.; Schlegel, H.B.; Bernhard Schlegel, H. Combining Synchronous Transit and Quasi-Newton Methods to Find Transition States. *Isr. J. Chem.* **1993**, *33*, 449–454. [CrossRef]
31. Mennucci, B.; Cancès, E.; Tomasi, J. Evaluation of solvent effects in isotropic and anisotropic dielectrics and in ionic solutions with a unified integral equation method: Theoretical bases, computational implementation, and numerical applications. *J. Phys. Chem. B* **1997**, *101*, 10506–10517. [CrossRef]

Disclaimer/Publisher's Note: The statements, opinions and data contained in all publications are solely those of the individual author(s) and contributor(s) and not of MDPI and/or the editor(s). MDPI and/or the editor(s) disclaim responsibility for any injury to people or property resulting from any ideas, methods, instructions or products referred to in the content.